Canadian Mineralogist
Vol. 29, pp. 995-1017 (1991)

METAMORPHIC PETROLOGY OF Fe–Zn–Mg–Al ALTERATION AT THE LINDA VOLCANOGENIC MASSIVE SULFIDE DEPOSIT, SNOW LAKE, MANITOBA*

EVA ZALESKI AND EDGAR FROESE
Geological Survey of Canada, 601 Booth Street, Ottawa, Ontario K1A 0E8

TERENCE M. GORDON
Department of Geology and Geophysics, University of Calgary, Calgary, Alberta T2N 1N4

ABSTRACT

Fe–Mg–Zn–Al alteration zones at the Linda deposit are characterized by metamorphic assemblages that include quartz, muscovite, pyrite, zincian staurolite, kyanite, gahnite, biotite, chlorite and sphalerite. These assemblages crystallized under amphibolite-facies conditions during syn-D_2 peak metamorphism. Analyses of sulfide, silicate and oxide minerals in low-variance assemblages were used to balance metamorphic reactions in the system Si–Al–Fe–Mg–Zn–K–H–F–O–S. Chemographic analysis of assemblages containing quartz, muscovite and pyrite defines a log $f(S_2)$ – log $f(O_2)$ petrogenetic grid at fixed pressure, temperature, $f(H_2O)$ and f(HF). The mineral assemblages can be represented in the subsystem Mg–Zn–Al_2. Reactions involving four Mg–Zn–Al_2 minerals define univariant curves; equilibrium compositions of coexisting minerals vary along the curves. Assemblages containing chlorite – kyanite or biotite – kyanite can be modeled in a Zn-absent subsystem by isopleths of Fe end-member activity in continuous sulfidation–oxidation reactions. Fluorine occurs in significant amounts in biotite at the Linda deposit. As a result of Fe–F avoidance, biotite is higher in Mg/(Mg+Fe) than coexisting chlorite. The reversal in Fe–Mg partitioning modifies reaction topology, and biotite – kyanite is stable at higher $f(S_2)$ than chlorite. Sphalerite geobarometry indicates a maximum pressure during syn-D_2 metamorphism of about 5 kbar. The coexistence of Fe-rich staurolite + quartz and margarite + quartz constrains the temperature of peak metamorphism to about 550°C, consistent with the chlorite – biotite – staurolite zone in pelitic metasedimentary rocks. In the metamorphosed altered rocks, the assemblages staurolite – anthophyllite and biotite – kyanite, which would normally crystallize at higher grade, were stabilized by Zn and F, respectively. The presence of Zn and F, and the reversed Fe–Mg partitioning between biotite and chlorite, invalidate the application of P–T grids derived for pelitic bulk-rock compositions. Metamorphic isograds in the Snow Lake region require a reinterpretation that takes into account the composition of a hydrothermally altered protolith.

Keywords: sulfidation–oxidation equilibria, zincian staurolite, gahnite, Fe–F avoidance, partitioning reversal, Snow Lake, Manitoba.

SOMMAIRE

Les zones d'altération du gisement Linda, au lac Snow (Manitoba), contiennent des assemblages métamorphiques à quartz, muscovite, pyrite, staurotide zincifère, kyanite, gahnite, biotite, chlorite et sphalérite. Ces assemblages ont cristallisé dans le facies amphibolite lors du paroxysme métamorphique syn-D_2. Les résultats d'analyses des sulfures, silicates et oxydes des assemblages à faible variance ont été utilisés pour balancer les réactions métamorphiques dans le système Si–Al–Fe–Mg–Zn–K–H–F–O–S. L'analyse chimiographique des assemblages à quartz, muscovite et pyrite définit une grille pétrogénétique en termes de log $f(S_2)$ – log $f(O_2)$ à pression, température, $f(H_2O)$ et f(HF) constantes. On peut représenter les assemblages de minéraux dans le sous-système Mg–Zn–Al_2. Les réactions impliquant quatre minéraux à Mg–Zn–Al_2 définissent des courbes univariantes; les compositions des minéraux à l'équilibre varient le long des courbes. Les assemblages à chlorite – kyanite ou à biotite – kyanite peuvent être reproduits dans un sous-système sans Zn, par des courbes d'activité constante du pôle ferrifère dans les réactions continues de sulfuration et d'oxydation. Le fluor est présent en quantités importantes dans la biotite de ce gisement. Vue l'instabilité relative des liaisons Fe–F, la biotite est plus riche en Mg/(Mg+Fe) que la chlorite coexistante. L'inversion dans la distribution Fe–Mg modifie la topologie réactionnelle, et la paire biotite – kyanite est stable à une valeur de $f(S_2)$ plus élevée que la chlorite. La géobarométrie fondée sur la sphalérite indique une pression maximale pendant le métamorphisme syn-D_2 d'environ 5 kbar. La coexistence des paires staurotide ferrifère – quartz et margarite – quartz limite la température maximale du métamorphisme à environ 550°C, ce qui concorde avec la zone à chlorite – biotite – staurotide dans les roches pélitiques métasédimentaires.

*Lithoprobe Publication No. 219; Geological Survey of Canada contribution number 57990.

Dans les roches altérées métamorphisées, les assemblages staurotide – anthophyllite et biotite – kyanite, qui apparaissent normalement à un niveau métamorphique plus élevé, ont été stabilisés par le Zn et le F, respectivement. La présence de Zn et F, et l'inversion dans la distribution Fe–Mg entre la biotite et la chlorite, rendent invalides l'application des grilles P–T dérivées à partir des roches à compositions pélitiques. Les isogrades métamorphiques dans la région du lac Snow exigent une réinterprétation qui tient compte de la composition des roches dont la composition a été modifiée par une altération hydrothermale.

Mots-clés: équilibres de sulfuration et d'oxydation, staurotide zincifère, gahnite, incompatibilité Fe–F, coefficient de distribution inversé, lac Snow, Manitoba.

INTRODUCTION

The conceptual framework needed to model metamorphic silicate – oxide – sulfide equilibria is still evolving. In Fe–Mg minerals, progressive sulfidation or oxidation of Fe end-members produces progressively more magnesian compositions (Bryndzia & Scott 1987, Froese 1971, 1977, Mohr & Newton 1983, Nesbitt 1982, 1986a, b). However, at the Linda deposit, the presence of Zn and F in altered rocks results in more complex phase-relations among the Fe–Mg phyllosilicates, Fe–Zn–Mg-bearing staurolite and gahnite, and Zn–Fe-bearing sphalerite.

In this contribution, we have taken into account ternary Fe–Zn–Mg solutions in gahnite and staurolite in the treatment of silicate – oxide – sulfide assemblages. The approach is initially empirical; we make use of electron-microprobe data on the composition of minerals in low-variance assemblages to balance reactions, and we use chemographic analysis to develop petrogenetic grids as functions of S_2 and O_2 fugacities, pressure and temperature. Mineral abbreviations are from Kretz (1983), with the following exceptions: Al-sil for aluminosilicate, bi for biotite, ch for chlorite, da for daphnite, gh for gahnite, hpo for hexagonal pyrrhotite, il for ilmenite, mg for magnetite, mpo for monoclinic pyrrhotite, ru for rutile, si for sillimanite, sid for siderophyllite, and xn for xenotime.

REGIONAL GEOLOGY

The Linda deposit is located in the Snow Lake region of the Flin Flon – Snow Lake volcanic belt (Fig. 1), in the Proterozoic Trans-Hudson Orogen. The volcanic belt is flanked by the Kisseynew gneiss belt to the north, and to the south, it is overlain by Paleozoic sedimentary rocks. The following brief summary of the regional geology of Snow Lake (Fig. 1) is based mainly on Froese & Moore (1980).

Supracrustal rocks have been divided into two groups, Amisk and Missi. The Amisk Group encompasses a suite of intercalated mafic and felsic metavolcanic rocks, and overlying metasedimentary rocks, mainly greywackes and shales. Amisk metasedimentary rocks (ornamented in Fig. 1) have pelitic bulk-compositions and commonly contain mineral assemblages definitive of regional metamorphic grade. The Missi Group, which was deposited on Amisk Group rocks, consists mainly of metamorphosed lithic arenites.

The Linda deposit is one of several volcanogenic massive sulfide deposits in the Snow Lake region. It is subeconomic and contains massive and disseminated pyritic mineralization with minor amounts of pyrrhotite, sphalerite and chalcopyrite. Economic Cu–Zn deposits in the vicinity include the mines at Anderson Lake, Stall Lake and Rod. The deposits are hosted by Amisk felsic volcanic rocks and are associated with extensive zones of synvolcanic hydrothermal alteration. The altered rocks are characterized by assemblages of amphibolite-facies metamorphic minerals that resulted from the regional dynamometamorphic overprinting of altered protoliths (Bailes 1987, 1988, Froese & Moore 1980, Walford & Franklin 1982, Zaleski & Halden 1988).

Froese & Moore (1980) proposed three deformational events. D_1 produced tight to isoclinal F_1 folds. The McLeod Road thrust fault (Fig. 1), although locally showing evidence of late reactivation (Galley *et al.* 1988), is a probable pre-D_1 or syn-D_1 fault. D_2 produced northeasterly trending flexural folds. D_3 deformation was restricted to the northern part of the Snow Lake region.

Metamorphic assemblages in the Flin Flon – Snow Lake belt show a transition from a low-grade metavolcanic terrane in the south, to the high-grade Kisseynew gneiss belt in the north (Froese & Gasparrini 1975, Froese & Moore 1980). In the Snow Lake region, metamorphic isograds delineate four metamorphic zones characterized by the assemblages: chlorite – biotite, chlorite – biotite – staurolite, biotite – staurolite – sillimanite and biotite – sillimanite – almandine (Fig. 1). Prograde isograd reactions (listed in Fig. 1) were inferred from parageneses in Amisk pelitic metasedimentary rocks.

The reaction assemblage for the biotite – sillimanite isograd (chlorite – staurolite – aluminosilicate – biotite – muscovite) is present in the altered rocks at the Anderson Lake and Stall Lake mines. The parageneses in altered rocks commonly resemble those of metapelites; hence the biotite – sillimanite isograd was mapped on the

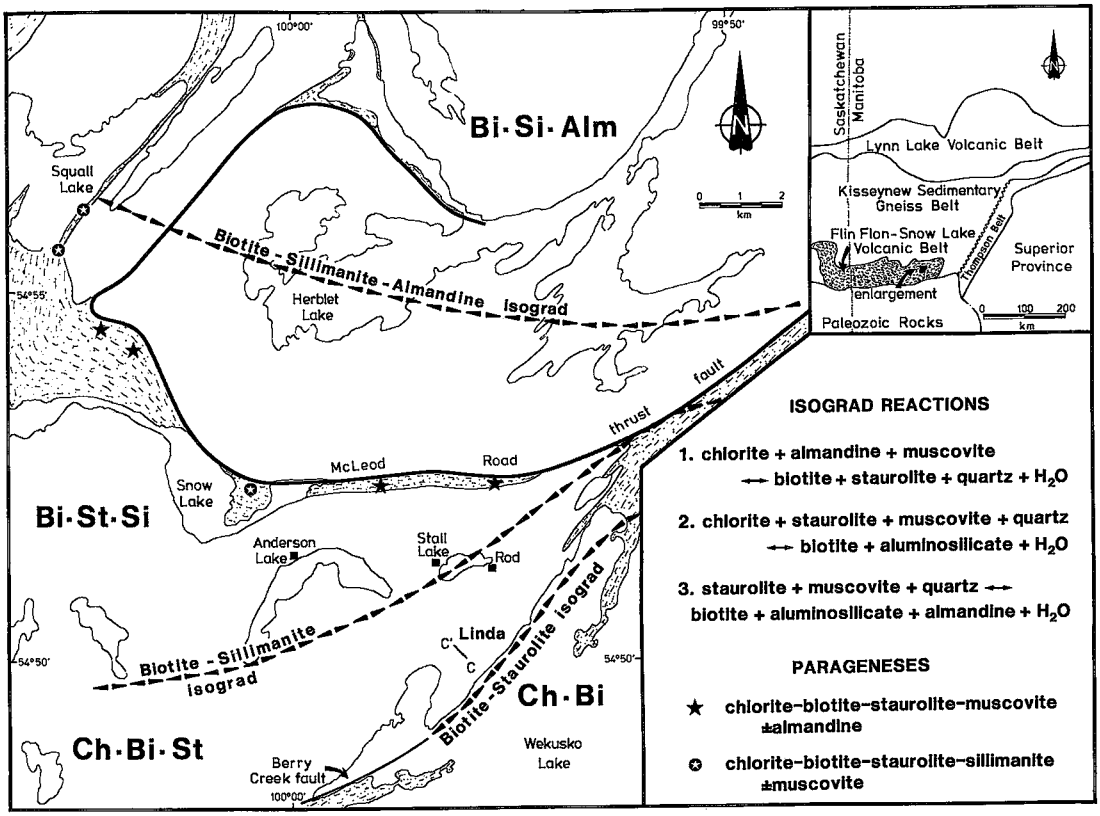

FIG. 1. Location (inset), regional metamorphic geology of Snow Lake, and isograd reactions (inset) based on Froese & Moore (1980). Metapelites belonging to the Amisk Group are ornamented. Stars mark the locations of assemblages of lower grade in pelitic rocks north of the biotite - sillimanite isograd. The location of subsurface cross-section C–C' of the Linda deposit (Fig. 2) is indicated by the bar.

basis of the first appearance of aluminosilicate, irrespective of the protolith (Froese & Moore 1980). Assemblages of lower grade (indicated by stars in Fig. 1) are present in metapelites to the north of the isograd. Chlorite in these assemblages was regarded as a retrograde mineral by Froese & Moore.

There is a dichotomy in the distribution of aluminosilicate polymorphs in the region; kyanite is present at Stall Lake, and both kyanite and sillimanite at Anderson Lake, whereas sillimanite is present in metapelites. The erosional surface was interpreted to expose an isobaric prograde sequence corresponding to the intersection of the biotite - aluminosilicate isograd reaction with the kyanite - sillimanite phase boundary (Froese & Moore 1980).

GEOLOGY OF THE LINDA AREA

The pyritic mineralization of the Linda deposit is hosted by felsic metavolcanic rocks that have undergone synvolcanic Fe-Mg-Zn-Al alteration (Fig. 2). The alteration is disposed in two discrete zones, designated as "proximal" and "distal" with reference to their relative distance from massive sulfide mineralization, and without lithofacial connotation (Zaleski 1989). The deposit is overturned, with the alteration zones overlying the massive sulfide bodies.

The distal zone defines a relatively homogeneous zone of Na and Ca depletion; the most common rock-type is a feldspar-absent staurolite-banded gneiss. It is enveloped by felsic rocks containing calc-silicate minerals, mainly epidote. The proximal zone is heterogeneous, encompassing graphitic and margarite-bearing metasediments, sulfidic muscovite-rich metasediments, massive sulfide bodies and altered felsic rocks. There is a single occurrence of quartz - staurolite - anthophyllite - gahnite rock in an enclave in the largest massive sulfide body (Fig. 2, 1131). Both the distal and proximal zones have an irregular Zn-rich core characterized by

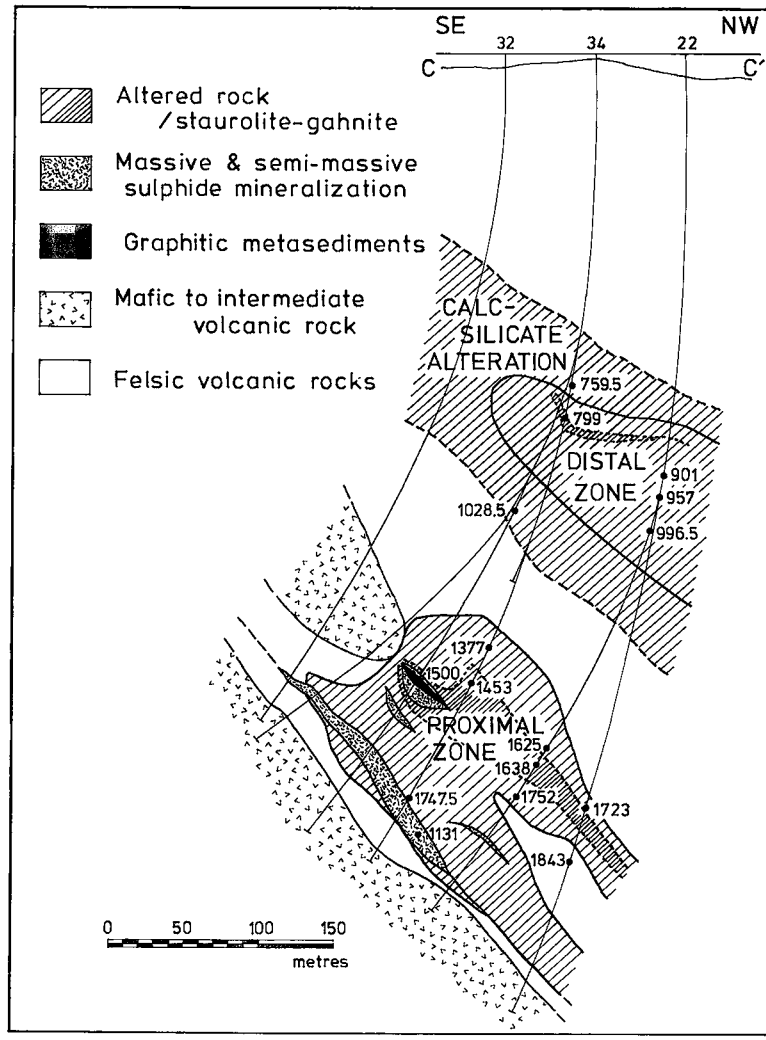

FIG. 2. Cross-section C–C' of the Linda deposit looking southwest, with sample locations. Sample 1131 lies in an adjacent cross-section and was projected onto the C–C' plane. Horizontal and vertical scales are equal.

muscovite schists with zincian staurolite and gahnite.

In the Linda area, there is evidence of at least two episodes of deformation (Zaleski 1989, Zaleski & Halden 1991), and the planar tectonic fabrics, S_1 and S_2, are pertinent to this study. S_1 is defined by metamorphic segregation layering, flattening of primary features (*e.g.*, clasts, quartz phenocrysts), mineral schistosity and trails of inclusions. S_2 is most commonly a crenulation cleavage, but it also is defined by the orientation of (001) planes of biotite. Porphyroblastic minerals are mainly syn-kinematic with D_2. The observations indicating this are: skeletal crystals with habits mimetic after S_1 and S_2 cleavages but showing some misorientation with respect to S_2 in the matrix, and porphyroblasts containing S_1 inclusion trails and showing crystallographic orientation parallel to S_2. Garnet in altered rocks shows dimensional orientation and inclusion trails parallel to S_1 cleavage, indicating pre-D_2 and probably syn-D_1 growth of garnet.

Two generations of kyanite can be distinguished. Syn-D_1 kyanite shows crystallographic and dimensional orientation parallel to S_1 schistosity, and transposition and strain related to development of the S_2 fabric. Syn-D_2 kyanite occurs as skeletal crystals mimetic after S_1 and S_2 fabrics, as previously described for syn-D_2 porphyroblasts in

general. Syn-D_1 kyanite is not associated with biotite; syn-D_2 kyanite is associated with biotite, typically a nearly colorless phlogopite.

The Linda deposit lies in the chlorite – biotite – staurolite zone of regional metamorphism as based on parageneses in metapelites (Fig. 1). At the deposit, parageneses in altered volcanic rocks include muscovite – chlorite – biotite – garnet – staurolite and muscovite – chlorite – staurolite – biotite – kyanite; these are the reaction assemblages for the biotite – staurolite and biotite – aluminosilicate isograds, respectively. The assemblage staurolite – anthophyllite, normally stable within the biotite – staurolite – sillimanite zone (Froese & Moore 1980), also is present. The relationship between the altered rocks and regional metamorphism is one of the major questions addressed in this study.

Mineral Chemistry

Method

The selection of samples for electron-microprobe analysis was aimed at representing the variety of low-variance silicate – oxide – sulfide assemblages in altered rocks (Fig. 2, Table 1). In particular, staurolite-bearing parageneses were represented. Mineral analyses were carried out on a JEOL Superprobe 733 at the Mineral Sciences Division, Canadian Museum of Nature, Ottawa. Mineral compositions are reported here for staurolite, gahnite, garnet, sphalerite, biotite, muscovite and chlorite (Table 2).

Mineral compositions were determined by wavelength-dispersion spectrometry (WDS) using an accelerating potential of 15 kV, a beam current of 20–25 nA, and a beam diameter of 10–16 μm. A focused beam was used for some very fine disseminated grains of sphalerite. Mineral standards were used, except for Zn in phyllosilicate minerals, for which synthetic $BaZnGeO_4$ was used as standard. For the analysis of phyllosilicates, the following mineral standards were used: chlorite for Si, Al and Mg, biotite for Ti, Fe and K, chromite for Cr, willemite for Mn, diopside for Ca, sanbornite for Ba, albite for Na, fluoriebeckite for F, and tugtupite for Cl. For staurolite, gahnite,

TABLE 1. SUMMARY OF MINERAL ASSEMBLAGES

a. DISTAL ALTERATION ZONE

Sample	Assemblages	Accessory Minerals
22-901	qtz, **ms**,[1] **ch, ky, st,** py, **sp.**	pl,[2] ap, aln, tur, zrn, ru, il.[3]
22-957	qtz, **ms, st, ch,** py.	**mrg,** grt, tur, sp, ap, aln, mg, il, ru, mnz, xn.
22-996.5	qtz, **ch, ms, st,** mg, py.	il, ap, aln.
34-799a	qtz, **ms, gh, st,** py, **sp.**	tur, **ch,**[4] ap, ccp, si,[4] ru.
34-799b	qtz, ms, **gh,** py, **sp.**	tur, ccp, ru, ch.[4]

b. PROXIMAL ALTERATION ZONE

Sample	Assemblages	Accessory Minerals
22A-1625	qtz, **ms, ch, st, grt, bi,** py, **sp.**	mpo,[3] tur, aln, ap, zrn, ccp, ru.
22A-1638	qtz, **ms, st, ky,** py, **gh, sp.**	**tur,** ap, zrn, po, ccp, ru.
22A-1752	qtz, **ms,** py, **ky, ch, st, bi.**	**pl,** tur, ru, ap, ccp.
22B-1723	qtz, **ms, st,** py, **gh, bi, sp.**	mrg, ap, tur, zrn, gn, ru, grn, **ch,**[4] cal.[3]
34C-1377	qtz, **ms, st,** py, **ky, bi, ch, sp.**	**pl, tur,** ap, zrn, ru, xn, si.[4]
34C-1453	qtz, **ms, st, gh,** py.	mpo,[3] **bi,**[4] **ch,**[4] ap, zrn, aln, ru, il, xn, mnz.
34C-1747.5	qtz, **ms, ky, st, bi,** py, hpo.	ap, mpo,[3] **ch,**[4] ccp, ru.
34-1500	qtz, gr, **ky,** py, hpo, **bi, ms,** sp.	mpo,[3] **mrg, ch,**[4] apy, ccp, tur.
24-1131	qtz, **st, ath,** py, **gh,** mg, hpo.	**pl,** mpo,[3] ccp, **bi,**[4] apy, si.[4]

[1] Analyzed minerals in boldface.
[2] Inferred from altered pseudomorphs.
[3] Retrograde.
[4] Not part of the equilibrium assemblage.

TABLE 2a. MUSCOVITE AND MARGARITE COMPOSITIONS

Sample	901 (6)*	1625 (2)	1638 (2)	1752 (2)	1723 (10)	799a (6)	1500ms	1500mrg (4)	1377 (3)	1747.5 (6)
SiO_2	45.73 (0.36)	45.81 (0.26)	44.68 (0.26)	46.73 (1.02)	45.17 (0.75)	45.25 (0.44)	46.73	31.08 (0.22)	46.82 (0.28)	45.82 (0.15)
TiO_2	0.40 (0.05)	0.47 (0.04)	0.32 (0.02)	0.29 (0.06)	0.41 (0.04)	0.35 (0.05)	0.00	0.08 (0.01)	0.36 (0.02)	0.31 (0.03)
Al_2O_3	36.12 (0.35)	36.53 (0.05)	36.28 (0.23)	35.46 (1.08)	36.30 (0.61)	36.77 (0.42)	36.80	50.96 (0.10)	37.03 (0.31)	36.70 (0.21)
FeO	2.09 (0.18)	1.32 (0.03)	0.80 (0.08)	1.17 (0.10)	1.56 (0.08)	1.20 (0.07)	0.00	0.07 (0.07)	1.20 (0.07)	1.65 (0.08)
MgO	0.65 (0.05)	0.76 (0.02)	0.59 (0.03)	0.61 (0.17)	0.80 (0.06)	0.58 (0.08)	1.22	0.27 (0.04)	0.81 (0.08)	0.64 (0.03)
BaO	0.17 (0.02)	0.17 (0.01)	0.12 (0.01)	0.02 (0.05)	0.10 (0.05)	0.13 (0.02)	0.48	0.00 (0.00)	0.08 (0.05)	0.07 (0.07)
CaO	0.00 (0.00)	0.00 (0.00)	0.00 (0.00)	0.00 (0.00)	0.75 (0.41)	0.02 (0.02)	0.04	11.09 (0.23)	0.00 (0.00)	0.00 (0.00)
Na_2O	1.54 (0.08)	1.59 (0.06)	2.07 (0.03)	2.30 (0.24)	0.98 (0.05)	1.68 (0.09)	0.78	0.64 (0.04)	1.47 (0.06)	1.65 (0.07)
K_2O	9.13 (0.19)	8.65 (0.15)	7.53 (0.25)	8.16 (0.49)	8.68 (0.33)	8.36 (0.17)	9.41	0.23 (0.06)	8.05 (0.19)	9.07 (0.22)
H_2O†	4.53 (0.03)	4.53 (0.02)	4.43 (0.01)	4.52 (0.05)	4.50 (0.04)	4.50 (0.03)	4.56	4.51 (0.02)	4.59 (0.03)	4.55 (0.01)
Total‡	100.35 (0.61)	99.82 (0.42)	96.80 (0.31)	99.26 (1.01)	99.24 (0.81)	98.82 (0.53)	100.02	98.92 (0.41)	100.40 (0.68)	100.45 (0.34)
Si	6.059 (0.019)	6.061 (0.011)	6.053 (0.008)	6.196 (0.117)	6.024 (0.077)	6.035 (0.041)	6.143	4.132 (0.015)	6.115 (0.004)	6.045 (0.016)
^{IV}Al	1.941 (0.019)	1.939 (0.011)	1.947 (0.008)	1.804 (0.117)	1.976 (0.077)	1.965 (0.041)	1.857	3.868 (0.015)	1.885 (0.004)	1.955 (0.016)
^{VI}Al	3.702 (0.034)	3.759 (0.003)	3.847 (0.005)	3.739 (0.049)	3.731 (0.020)	3.818 (0.019)	3.847	4.118 (0.011)	3.815 (0.008)	3.753 (0.008)
Ti	0.040 (0.005)	0.047 (0.004)	0.033 (0.005)	0.028 (0.006)	0.041 (0.004)	0.035 (0.005)	0.000	0.007 (0.002)	0.035 (0.002)	0.031 (0.003)
Fe	0.232 (0.020)	0.146 (0.003)	0.090 (0.001)	0.129 (0.011)	0.174 (0.009)	0.134 (0.008)	0.000	0.008 (0.008)	0.131 (0.008)	0.182 (0.009)
Mg	0.128 (0.009)	0.149 (0.002)	0.119 (0.004)	0.120 (0.035)	0.158 (0.012)	0.115 (0.015)	0.239	0.054 (0.007)	0.158 (0.016)	0.126 (0.005)
site	4.102 (0.010)	4.101 (0.002)	4.089 (0.006)	4.017 (0.029)	4.105 (0.018)	4.102 (0.015)	4.086	4.186 (0.024)	4.139 (0.012)	4.092 (0.015)
Ba	0.009 (0.001)	0.009 (0.001)	0.006 (0.001)	0.001 (0.002)	0.005 (0.003)	0.007 (0.001)	0.025	0.000 (0.000)	0.004 (0.003)	0.004 (0.004)
Ca	0.000 (0.000)	0.000 (0.000)	0.000 (0.000)	0.000 (0.000)	0.106 (0.058)	0.002 (0.003)	0.006	1.580 (0.028)	0.000 (0.000)	0.000 (0.000)
Na	0.396 (0.021)	0.407 (0.016)	0.544 (0.009)	0.591 (0.060)	0.252 (0.013)	0.434 (0.021)	0.199	0.165 (0.010)	0.371 (0.015)	0.421 (0.017)
K	1.543 (0.026)	1.460 (0.020)	1.301 (0.041)	1.380 (0.087)	1.477 (0.057)	1.422 (0.031)	1.578	0.038 (0.009)	1.342 (0.042)	1.527 (0.035)
site	1.947 (0.027)	1.876 (0.004)	1.851 (0.033)	1.973 (0.058)	1.841 (0.041)	1.864 (0.029)	1.807	1.783 (0.028)	1.717 (0.019)	1.951 (0.040)
H†	4.000	4.000	4.000	4.000	4.000	4.000	4.000	4.000	4.000	4.000
O	24.000	24.000	24.000	24.000	24.000	24.000	24.000	24.000	24.000	24.000

* In this and the following tables, the number of analyses and 1σ standard deviation are in parentheses.
† Calculated from stoichiometry. ‡ F, Cl, Mn and Cr not detected.

TABLE 2b. BIOTITE COMPOSITIONS

Sample	1625 (5)*	1752 (2)	1723 (5)	1500 (6)	1377 (5)	1747.5 (6)
SiO_2	37.87 (0.35)	38.40 (0.11)	37.15 (0.61)	41.68 (0.15)	39.82 (0.06)	37.34 (0.24)
TiO_2	1.02 (0.05)	1.00 (0.01)	1.27 (0.08)	0.34 (0.02)	0.72 (0.01)	1.18 (0.06)
Al_2O_3	19.19 (0.15)	18.92 (0.07)	18.79 (0.12)	17.21 (0.23)	18.50 (0.08)	18.69 (0.21)
FeO	10.75 (0.15)	9.73 (0.14)	14.32 (0.15)	1.30 (0.08)	9.04 (0.03)	13.79 (0.23)
MnO	0.24 (0.01)	0.20 (0.01)	0.17 (0.03)	0.05 (0.04)	0.28 (0.02)	0.11 (0.02)
MgO	17.52 (0.15)	19.34 (0.14)	15.61 (0.25)	25.25 (0.15)	19.75 (0.08)	15.72 (0.15)
BaO	0.00 (0.00)	0.00 (0.00)	0.00 (0.00)	0.16 (0.01)	0.00 (0.00)	0.00 (0.00)
CaO	0.00 (0.00)	0.02 (0.02)	0.03 (0.02)	0.01 (0.02)	0.00 (0.00)	0.00 (0.00)
Na_2O	0.41 (0.02)	0.38 (0.02)	0.28 (0.07)	0.33 (0.02)	0.41 (0.01)	0.40 (0.05)
K_2O	9.24 (0.43)	8.57 (0.38)	8.72 (0.22)	8.73 (0.47)	8.18 (0.21)	8.97 (0.27)
F	1.67 (0.15)	2.83 (0.08)	1.51 (0.09)	3.53 (0.13)	2.18 (0.15)	1.64 (0.13)
H_2O†	3.37 (0.08)	2.88 (0.05)	3.39 (0.05)	2.66 (0.05)	3.23 (0.08)	3.33 (0.07)
Total‡	100.57 (0.72)	101.06 (0.07)	100.62 (0.52)	99.76 (0.69)	101.17 (0.26)	100.48 (0.63)
Si	5.452 (0.022)	5.460 (0.006)	5.423 (0.060)	5.766 (0.016)	5.606 (0.005)	5.453 (0.028)
^{IV}Al	2.548 (0.022)	2.540 (0.005)	2.577 (0.060)	2.234 (0.016)	2.394 (0.005)	2.547 (0.028)
^{VI}Al	0.709 (0.011)	0.631 (0.003)	0.658 (0.033)	0.573 (0.037)	0.676 (0.005)	0.670 (0.028)
Ti	0.111 (0.004)	0.106 (0.001)	0.139 (0.009)	0.035 (0.002)	0.076 (0.001)	0.130 (0.006)
Fe	1.294 (0.022)	1.157 (0.014)	1.749 (0.024)	0.151 (0.010)	1.064 (0.003)	1.684 (0.025)
Mn	0.029 (0.001)	0.023 (0.001)	0.021 (0.003)	0.006 (0.005)	0.033 (0.002)	0.013 (0.002)
Mg	3.760 (0.042)	4.098 (0.025)	3.396 (0.070)	5.207 (0.022)	4.143 (0.020)	3.420 (0.041)
site	5.903 (0.044)	6.016 (0.042)	5.963 (0.060)	5.971 (0.018)	5.992 (0.018)	5.917 (0.025)
Ba	0.000 (0.000)	0.000 (0.000)	0.000 (0.000)	0.009 (0.001)	0.000 (0.000)	0.000 (0.000)
Ca	0.000 (0.000)	0.003 (0.003)	0.005 (0.003)	0.001 (0.002)	0.000 (0.000)	0.000 (0.000)
Na	0.114 (0.006)	0.105 (0.005)	0.079 (0.019)	0.087 (0.005)	0.112 (0.004)	0.113 (0.014)
K	1.697 (0.071)	1.555 (0.070)	1.624 (0.035)	1.541 (0.078)	1.469 (0.035)	1.671 (0.043)
site	1.811 (0.075)	1.662 (0.080)	1.709 (0.050)	1.639 (0.082)	1.581 (0.037)	1.784 (0.038)
F	0.759 (0.069)	1.273 (0.037)	0.695 (0.043)	1.545 (0.054)	0.971 (0.070)	0.757 (0.062)
H†	3.241 (0.069)	2.727 (0.037)	3.305 (0.043)	2.455 (0.054)	3.029 (0.070)	3.243 (0.062)
O	23.241	22.727	23.305	22.455	23.029	23.243

† Calculated from stoichiometry. ‡ Cl, Cr and Zn not detected.

garnet and kyanite, the following standards were used: almandine for Si and Fe, titanite for Ti, gehlenite for Al, nichromite for Cr, diopside for Mg and Ca, tephroite for Mn, willemite for Zn, and albite for Na. For sphalerite, the following standards were used: sphalerite for Zn and S, arsenopyrite for Fe, tephroite for Mn, cuprite for Cu, and Cd-bearing apatite for Cd. Data were processed with a conventional ZAF correction.

During calibration, counts on standards for major elements were collected to a minimum 1σ precision of 0.50%. Counts on samples were collected to a 1σ precision of 0.50%, or for maximum counting times of 25–40 seconds. The results of each analysis were recorded with the cumulative 1σ standard deviation for both standard and sample. Elements for which the standard deviation of sample counts exceeded 25.50% (relative error) were considered not detected. Cl was not detected in any samples. Detection limits for F were 0.39% in chlorite, 0.44% in biotite and 0.46% in muscovite. Detection limits for Zn were 0.16% in chlorite and less than 0.24% in biotite.

Results of chlorite analyses tend to have slightly high analytical totals; these average 101.26 to 102.00% after the addition of calculated H_2O. Biotite analyses also tend to have high sums, from 99.76 to 101.17%. This is probably due to a systematic error introduced during calibration on the standards and may be related to either the choice of standards or to inaccuracy in the reported compositions. Chlorite and biotite standards were used for major elements to minimize the differences in matrix between the standards and the minerals analyzed. The element(s) in which the systematic error occurs cannot be definitely identified, and this will contribute to the uncertainty of the analyses. Interpretations relying on relative magnitude should not be affected.

Recasting of analyses (except in the case of staurolite) to structural formulae followed the method of Deer *et al.* (1966). The proportion of

TABLE 2c. CHLORITE COMPOSITIONS

Sample	901 (6)*	1625 (4)	1752 (6)	1377 (5)
SiO_2	25.30 (0.40)	26.30 (0.53)	26.29 (0.22)	26.59 (0.31)
TiO_2	0.04 (0.03)	0.07 (0.01)	0.05 (0.03)	0.05 (0.03)
Al_2O_3	24.44 (0.28)	24.52 (0.60)	24.34 (0.28)	24.46 (0.21)
FeO	20.59 (0.16)	14.73 (0.18)	15.23 (0.46)	13.01 (0.18)
MnO	0.30 (0.02)	0.43 (0.01)	0.38 (0.02)	0.50 (0.01)
MgO	19.32 (0.21)	22.72 (0.43)	23.20 (0.29)	24.51 (0.34)
ZnO	0.00 (0.00)	0.11 (0.11)	0.00 (0.00)	0.00 (0.00)
Na_2O	0.00 (0.00)	0.02 (0.03)	0.00 (0.00)	0.00 (0.00)
K_2O	0.01 (0.00)	0.16 (0.18)	0.02 (0.04)	0.03 (0.05)
F	0.00 (0.00)	0.00 (0.00)	0.36 (0.27)	0.30 (0.25)
H_2O†	12.00 (0.04)	12.23 (0.12)	12.11 (0.10)	12.22 (0.10)
Total‡	102.00 (0.30)	101.26 (0.90)	101.82 (0.50)	101.54 (0.74)
Si	5.055 (0.075)	5.156 (0.060)	5.135 (0.033)	5.157 (0.028)
^{IV}Al	2.945 (0.075)	2.844 (0.060)	2.865 (0.033)	2.843 (0.028)
^{VI}Al	2.810 (0.022)	2.823 (0.116)	2.741 (0.039)	2.751 (0.029)
Ti	0.006 (0.004)	0.010 (0.001)	0.007 (0.005)	0.008 (0.004)
Fe	3.441 (0.035)	2.415 (0.044)	2.488 (0.074)	2.110 (0.035)
Mn	0.051 (0.004)	0.072 (0.001)	0.063 (0.003)	0.082 (0.002)
Mg	5.752 (0.058)	6.642 (0.187)	6.753 (0.087)	7.084 (0.041)
Zn	0.000 (0.000)	0.015 (0.016)	0.000 (0.000)	0.000 (0.000)
Na	0.000 (0.000)	0.007 (0.011)	0.000 (0.000)	0.000 (0.000)
K	0.002 (0.000)	0.038 (0.045)	0.004 (0.009)	0.006 (0.013)
site	12.062 (0.044)	12.023 (0.054)	12.057 (0.019)	12.042 (0.006)
F	0.000	0.000	0.223 (0.164)	0.185 (0.151)
H†	16.000	16.000	15.777 (0.164)	15.815 (0.151)
O	36.000	36.000	35.777	35.815

† Calculated from stoichiometry.
‡ Cl, Cr, Ba and Ca not detected.

H_2O was back-calculated from stoichiometry, after adjustment for F content. Staurolite formulae were normalized to (Si + Al) = 25.53, after the proposed scheme of Holdaway *et al.* (1986, 1988) for staurolite that formed under reducing conditions. Oxygen was assumed to total 48 atoms, and excess anionic charges were balanced by H^+. Li_2O was not determined, and the weight % of H_2O was back-calculated from the charge balance. The assignment of cations to structural sites, based on Holdaway *et al.* (1986), includes 0.250 Fe^{3+} at the octahedral Al(3A) sites, (Mn + Fe^{2+}) = 0.250 at the U(1) site, and Mg, Zn, Ti and the remaining Fe at the tetrahedral (Fe) site. The weight percents of Fe_2O_3 and adjusted FeO were back-calculated. This method produces oxide totals averaging 97.52 to 99.58%.

In general, the samples achieved equilibrium at the thin section scale, as inferred from the low-level random scatter of analytical values. Most analyses are reported as within-sample means (*i.e.*, within thin section) with 1σ standard deviations from the mean (Table 2). In most cases, mean values were used in balancing model reactions. Staurolite and gahnite show minor differences between core and rim compositions. In cases of systematic variation, average rim compositions were used. Garnet shows strong Fe–Mn zoning, and rim compositions were used to balance reactions. Sphalerite formulae were normalized to S = 1 before calculating balanced reactions.

Staurolite, gahnite and sphalerite

Staurolite and gahnite compositions span a wide range of Fe–Zn substitution, with minor variation in Mg (Fig. 3). The Zn content of staurolite is partly a function of bulk-rock composition; the compositional gap (between samples 1453 and 1721) is probably due to a gap in the bulk-rock compositions of the sample suite. The Mg content of staurolite and the Zn/Fe ratio of gahnite are mainly functions of S_2 and O_2 fugacities, as inferred from the coexisting Fe–Ti oxide and sulfide minerals.

TABLE 2d. STAUROLITE COMPOSITIONS

Sample	901 (4)* core	901 (4) rim	1625 (6)	1638 (6)	1752 (6)	1723 (6)	799a (6)	1377 (3) core	1377 (3) rim	1747.5 (6)
SiO_2	27.10 (0.11)	27.38 (0.14)	26.66 (0.29)	26.76 (0.62)	27.08 (0.23)	26.73 (0.16)	26.84 (0.29)	26.71 (0.18)	26.67 (0.27)	26.87 (0.18)
TiO_2	0.45 (0.03)	0.48 (0.04)	0.46 (0.09)	0.40 (0.05)	0.45 (0.05)	0.42 (0.03)	0.38 (0.03)	0.39 (0.05)	0.37 (0.02)	0.48 (0.07)
Al_2O_3	53.86 (0.53)	53.41 (0.31)	54.02 (0.35)	54.44 (0.51)	53.67 (0.47)	53.27 (0.42)	54.27 (0.58)	53.68 (0.28)	53.29 (0.50)	53.78 (0.39)
Fe_2O_3†	1.18	1.18	1.18	1.18	1.18	1.17	1.18	1.17	1.16	1.17
FeO	10.58 (0.29)	10.21 (0.18)	6.98 (0.23)	5.33 (0.12)	6.95 (0.37)	7.09 (0.10)	5.47 (0.34)	6.13 (0.07)	6.18 (0.05)	9.96 (0.22)
MnO	0.65 (0.04)	0.61 (0.03)	0.86 (0.03)	0.54 (0.02)	0.74 (0.03)	0.58 (0.03)	0.23 (0.02)	1.00 (0.02)	1.03 (0.04)	0.40 (0.04)
MgO	1.97 (0.05)	1.90 (0.05)	2.27 (0.08)	2.19 (0.06)	2.07 (0.17)	2.05 (0.06)	1.90 (0.24)	2.52 (0.09)	2.23 (0.07)	2.08 (0.13)
ZnO	1.21 (0.06)	1.12 (0.03)	4.83 (0.28)	6.91 (0.13)	3.94 (0.33)	6.15 (0.09)	7.16 (0.17)	5.21 (0.03)	5.23 (0.10)	1.58 (0.02)
H_2O†	1.70 (0.16)	1.77 (0.07)	1.64 (0.09)	1.83 (0.13)	1.91 (0.11)	1.41 (0.07)	1.89 (0.15)	1.61 (0.04)	1.68 (0.06)	1.77 (0.16)
Total‡	97.52 (0.36)	98.06 (0.37)	98.90 (0.19)	99.58 (0.41)	97.99 (0.70)	98.87 (0.47)	99.32 (1.07)	98.42 (0.28)	97.84 (0.79)	98.09 (0.37)
Si	7.637 (0.073)	7.737 (0.056)	7.533 (0.086)	7.513 (0.160)	7.651 (0.060)	7.622 (0.066)	7.545 (0.065)	7.578 (0.053)	7.609 (0.044)	7.598 (0.033)
^{IV}Al	0.363 (0.073)	0.263 (0.056)	0.467 (0.086)	0.487 (0.160)	0.349 (0.060)	0.378 (0.066)	0.455 (0.065)	0.422 (0.053)	0.391 (0.044)	0.402 (0.033)
^{VI}Al	17.530	17.530	17.530	17.530	17.530	17.530	17.530	17.530	17.530	17.530
Fe^{3+}†	0.250	0.250	0.250	0.250	0.250	0.250	0.250	0.250	0.250	0.250
Mn	0.155 (0.009)	0.146 (0.008)	0.207 (0.007)	0.129 (0.004)	0.178 (0.008)	0.141 (0.006)	0.056 (0.004)	0.240 (0.006)	0.249 (0.012)	0.096 (0.010)
Fe^{2+}	0.095 (0.009)	0.104 (0.008)	0.043 (0.008)	0.121 (0.004)	0.072 (0.008)	0.109 (0.006)	0.194 (0.004)	0.010 (0.006)	0.001 (0.012)	0.154 (0.010)
Ti	0.096 (0.008)	0.102 (0.009)	0.098 (0.019)	0.085 (0.012)	0.096 (0.009)	0.090 (0.006)	0.081 (0.007)	0.084 (0.011)	0.080 (0.006)	0.103 (0.015)
Fe^{2+}	2.400 (0.073)	2.309 (0.040)	1.606 (0.060)	1.090 (0.109)	1.570 (0.087)	1.582 (0.025)	1.091 (0.076)	1.444 (0.024)	1.473 (0.027)	2.203 (0.069)
Mg	0.825 (0.026)	0.799 (0.022)	0.954 (0.033)	0.917 (0.028)	0.870 (0.072)	0.873 (0.025)	0.795 (0.096)	1.065 (0.033)	0.947 (0.031)	0.877 (0.060)
Zn	0.251 (0.013)	0.223 (0.007)	1.007 (0.061)	1.433 (0.034)	0.822 (0.067)	1.296 (0.014)	1.485 (0.041)	1.091 (0.007)	1.102 (0.019)	0.330 (0.003)
site	3.572 (0.108)	3.443 (0.061)	3.665 (0.051)	3.525 (0.150)	3.358 (0.085)	3.840 (0.044)	3.452 (0.133)	3.683 (0.007)	3.601 (0.036)	3.513 (0.127)
H†	3.187 (0.283)	3.333 (0.137)	3.099 (0.159)	3.427 (0.218)	3.602 (0.208)	2.679 (0.117)	3.550 (0.298)	3.048 (0.058)	3.188 (0.101)	3.330 (0.286)
O	48.000	48.000	48.000	48.000	48.000	48.000	48.000	48.000	48.000	48.000

† Assumed or calculated from stoichiometry. ‡ Cr, Na and Ca not detected.

TABLE 2e. SPHALERITE COMPOSITIONS

Sample	1625 (2)*	1638 (7)	1723 (2)	799b (2)	799a	1377
Fe	7.76 (0.09)	6.36 (0.29)	8.36 (0.10)	7.26 (0.09)	5.27	2.44
Mn	0.41 (0.03)	0.03 (0.05)	0.15 (0.03)	0.00 (0.00)	0.00	0.00
Zn	57.88 (0.34)	60.59 (0.44)	57.58 (0.37)	58.54 (0.34)	60.56	65.85
Cd	0.24 (0.12)	0.00 (0.00)	0.47 (0.15)	1.10 (0.08)	0.00	0.00
Cu	0.07 (0.04)	0.02 (0.04)	0.20 (0.04)	0.21 (0.04)	0.00	0.00
S	33.15 (0.29)	33.27 (0.17)	32.87 (0.38)	33.53 (0.34)	34.32	31.75
Total	99.51 (0.45)	100.27 (0.45)	99.63 (0.79)	100.64 (0.09)	100.06	100.04
Fe	0.139 (0.002)	0.114 (0.005)	0.150 (0.002)	0.130 (0.002)	0.094	0.044
Mn	0.007 (0.001)	0.001 (0.001)	0.003 (0.001)	0.000 (0.000)	0.000	0.000
Zn	0.885 (0.005)	0.927 (0.007)	0.881 (0.006)	0.896 (0.005)	0.926	1.007
Cd	0.002 (0.001)	0.000 (0.000)	0.004 (0.001)	0.010 (0.001)	0.000	0.000
Cu	0.001 (0.001)	0.000 (0.001)	0.003 (0.001)	0.003 (0.001)	0.000	0.000
site	1.035 (0.009)	1.042 (0.007)	1.040 (0.010)	1.038 (0.008)	1.021	1.051
S	1.034 (0.009)	1.038 (0.005)	1.025 (0.012)	1.046 (0.001)	1.067	0.990

TABLE 2f. GAHNITE COMPOSITIONS

Sample	1638 (5)*	1723 (7)	799a (3)	799b (6)
SiO_2	0.02 (0.03)	0.03 (0.04)	0.25 (0.35)	0.06 (0.09)
Al_2O_3	59.02 (0.70)	58.62 (0.38)	58.71 (0.51)	58.31 (0.61)
FeO	5.01 (0.14)	7.27 (0.30)	5.38 (0.13)	5.10 (0.37)
MnO	0.15 (0.01)	0.23 (0.02)	0.03 (0.04)	0.00 (0.00)
MgO	2.39 (0.09)	2.44 (0.20)	2.04 (0.10)	2.12 (0.33)
ZnO	32.67 (0.28)	31.13 (0.63)	32.88 (0.13)	34.00 (0.90)
Total‡	99.26 (0.72)	99.72 (0.28)	99.29 (0.26)	99.59 (0.39)
Si	0.000 (0.001)	0.001 (0.001)	0.007 (0.010)	0.002 (0.003)
^{IV}Al	2.040 (0.005)	2.023 (0.005)	2.033 (0.012)	2.025 (0.005)
site	2.040 (0.005)	2.024 (0.005)	2.040 (0.005)	2.027 (0.005)
Fe	0.123 (0.003)	0.178 (0.007)	0.132 (0.004)	0.126 (0.008)
Mn	0.004 (0.000)	0.006 (0.001)	0.001 (0.001)	0.000 (0.000)
Mg	0.105 (0.004)	0.106 (0.009)	0.089 (0.005)	0.093 (0.014)
Zn	0.707 (0.010)	0.673 (0.016)	0.713 (0.003)	0.740 (0.025)
site	0.939 (0.008)	0.963 (0.007)	0.935 (0.009)	0.958 (0.008)
O	4.000	4.000	4.000	4.000

‡ Ti and Cr not detected.

Staurolite in the assemblage staurolite – anthophyllite – gahnite (1131) has a zincian composition.

Figure 3b focuses on the compositions of coexisting staurolite and gahnite. The staurolite compositions include only Fe^{2+} calculated at the tetrahedral Fe-bearing site, using the structural formula of Holdaway *et al.* (1986, 1988). Reactions (Table 3) involving staurolite were balanced using (Fe^{2+} + Fe^{3+}) on all sites.

Figure 3b portrays cation exchange involving only tetrahedral sites. The change in tie-line orientation correlates with Zn/Fe^{2+} in staurolite and may reflect nonideal mixing at tetrahedral sites. Al_2/Mg in staurolite shows little variation through a wide range of Zn/Fe (see Model mineral reactions), which supports the proposal that Fe and Mg are not completely exchangeable in staurolite (Grambling 1983).

TABLE 2g. GARNET COMPOSITIONS

Sample	1625 (3)* rim	1625 core
SiO_2	36.57 (0.09)	35.95
TiO_2	0.00 (0.00)	0.17
Al_2O_3	21.29 (0.12)	20.76
FeO	19.67 (0.17)	14.46
MnO	15.90 (0.08)	22.80
MgO	3.16 (0.05)	1.71
CaO	2.15 (0.10)	2.42
Na_2O	0.00 (0.00)	0.07
Total‡	98.80 (0.22)	98.40
Si	5.941 (0.010)	5.931
^{IV}Al	0.059 (0.010)	0.069
^{VI}Al	4.019 (0.010)	3.968
Ti	0.000 (0.000)	0.021
site	4.019 (0.010)	3.989
Fe	2.672 (0.015)	1.995
Mn	2.187 (0.013)	3.186
Mg	0.766 (0.009)	0.420
Ca	0.375 (0.015)	0.428
Na	0.000 (0.000)	0.022
site	6.000 (0.017)	6.052
O	24.000	24.000

‡ Cr not detected.

The range of Fe/Zn in sphalerite may reflect S_2 fugacity, but it is at least partly due to retrograde exchange. Some very fine grains approach end-member ZnS. In samples containing pyrrhotite, the low-temperature monoclinic polymorph is present, either with or without hexagonal pyrrhotite. The most Fe-rich sphalerite (1723) contains 14.5 mol% FeS and is associated with pyrite and syn-D_2 porphyroblastic minerals. Although some sphalerite compositions do not represent equilibrium, in practice, reaction coefficients (Table 3) are insensitive to sphalerite composition within the range allowed by equilibration with S_2 in the pyrite field.

Garnet

Strong compositional zoning in garnet is defined primarily by Mn–Fe substitution. In coarse porphyroblasts in sample 1625, the proportion of spessartine and almandine end-members, respectively, is 52.9 and 32.3 mol% in the core, and 36.3 and 44.9 mol% in the rim. Rim compositions were assumed to have equilibrated with syn-D_2 porphyroblasts.

Kyanite

Kyanite shows very slight deviation from ideal end-member composition, involving minor substitution of Fe^{3+} for Al to a maximum of 1.2% of the site.

Phyllosilicate minerals

Muscovite, margarite, chlorite and biotite are present in altered rocks. Margarite has nearly end-member composition (Table 2a, 1500 mrg). Muscovite has a Na/(Na + K) of 0.08 to 0.26 and contains a minor proportion of the celadonite end-member. Biotite compositions are Mg-rich; $Mg/(Fe_t + Mg)$ ranges from 0.55 to 0.98 and, in most cases, the mica can be classified as phlogopite. The most magnesian composition occurs in graphitic metasediment (1500), in which the mica approaches end-member phlogopite. Chlorite compositions also are magnesian and range in $Mg/(Fe_t + Mg)$ from 0.56 to 0.93. They correspond to high-Mg ripidolite and sheridanite, using the classification of Foster (1962).

Zn was detected sporadically in minor amounts (less than or equal to 0.26% ZnO) in chlorite (in 3 samples) and in biotite (1 sample). The values are not significant with respect to within-sample standard deviations at the 2σ level. There is no evidence of zincian chlorite, such as that described at Franklin, New Jersey (up to 9.60% ZnO, Frondel & Ito 1975).

Biotite commonly contains F at the hydroxyl site, from 0.86 to 3.77 wt.% F for biotite in the proximal alteration zone (Table 2b). Phlogopite in a graphitic metasediment (1500) contains the most F. Minor amounts of F, close to the detection limit, were detected in some cases in chlorite. F was not detected in muscovite that coexists with F-bearing biotite.

Fluorine and Fe–Mg partitioning

The F content of hydrous minerals generally shows a strong positive correlation with Mg/(Mg + Fe) (Guidotti 1984, Gunow *et al.* 1980, Munoz 1984) as a consequence of "Fe-F" avoidance, an electronic bonding phenomenon in transition metals (Valley *et al.* 1982) that results in the coupled

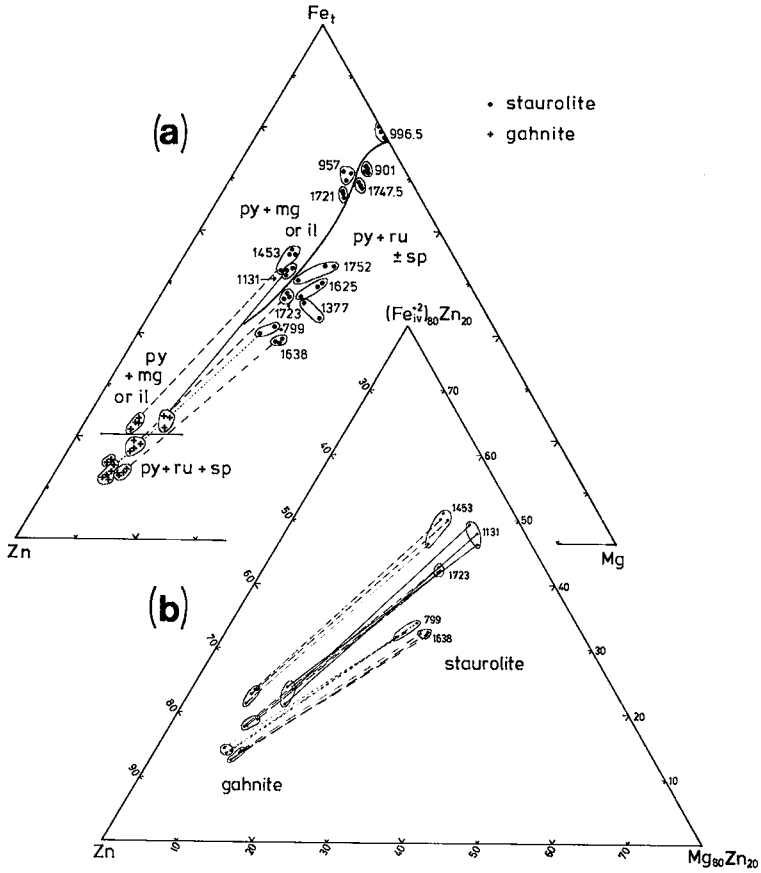

FIG. 3. Compositions of staurolite and gahnite. (a) Zn–Fe_t–Mg (molar proportions). Each point represents 1–3 analyses; ornamented tie-lines link the compositional fields for each sample. The dividing line separates assemblages coexisting with pyrite (py) and either magnetite (mg) or ilmenite (il), from assemblages coexisting with pyrite + rutile (ru) ± sphalerite (sp). Pyrrhotite occurs in some samples on both sides of the line. Fe_t is total Fe. (b) Zn–$^{IV}Fe^{2+}$–Mg (molar proportions) in coexisting staurolite and gahnite, with ornamented tie-lines linking compositions from within the same area. Only Fe^{2+} (calculated) at the tetrahedral Fe-bearing site was included; Fe^{3+} and Fe^{2+} at the Mn-bearing U(1) site were omitted. Samples 1638, 1723 and 799 contain sphalerite.

substitution, (Fe,OH) = (Mg,F). Munoz (1984) derived F-intercept values [$IV(F)_{bi}$] to compensate for the compositional dependency and to allow the expression of the degree of F enrichment as an independent parameter. The F-intercept value for biotite was formulated as: $IV(F)_{bi} = 1.52X_{Mg} + 0.42X_{ann} + 0.20X_{sid} - \log X_F/X_{OH}$, in which X_{Mg} is the mole fraction of Mg in the octahedral site, X_{ann} is the mole fraction of annite [$1 - (X_{Mg} + X_{sid})$], and X_{sid} is the mole fraction of siderophyllite [$(3 - Si/Al)/1.75(1-X_{Mg})$]. At fixed temperature, $IV(F)_{bi}$ is proportional to $\log f(H_2O)/f(HF)$ in the coexisting fluid [$\log f(H_2O)/f(HF) = 2100/T + IV(F)_{bi}$; Gunow *et al.* 1980]; thus, smaller values of $IV(F)_{bi}$ correlate with greater degrees of F enrichment.

Figure 4a shows the relationship between F and Mg/(Mg + Fe) in biotite at the Linda deposit, and Figure 4b shows the same data with F expressed as F-intercept values. The inner scale (Fig. 4b) shows values of $\log f(H_2O)/f(HF)$ in coexisting fluids calculated at an assumed temperature of 550°C. Biotite from the proximal zone of alteration equilibrated with fluids of relatively low ratio of H_2O/HF fugacity; biotite that coexists with kyanite invariably equilibrated with F-rich fluids.

TABLE 3. MODEL MINERAL REACTIONS

a. THE Si-Al-Fe-Mg-Zn-K-H-F-O-S SYSTEM

	Sample	Reaction	m[1]
1.	22-901	$8.47ky + 0.14ch + 2.14py + 0.27sp + 0.55H_2O + 1.27O_2 \rightleftharpoons st + 1.46qtz + 2.28S_2$	1.79
2.	22A-1638[2]	$st + 5.41sp + 2.17O_2 \rightleftharpoons 8.83gh + 7.51qtz + 0.96py + 1.71H_2O + 1.74S_2$	0.80
3.	22A-1752	$qtz + 2.36ky + 0.74bi + 0.33py + 4.52H_2O + 0.17O_2 \rightleftharpoons 0.44ch + 0.84ms + 0.85HF + 0.33S_2$	2.00
4.	22B-1723[2]	$st + 5.50sp + 2.12O_2 \rightleftharpoons 8.85gh + 7.61qtz + 1.15py + 1.34H_2O + 1.58S_2$	0.75
5.	34-799a[2]	$st + 5.42sp + 2.43O_2 \rightleftharpoons 8.98gh + 7.48qtz + 0.85py + 1.78H_2O + 1.86S_2$	0.76
6.	34C-1377	$qtz + 3.84ky + 1.22bi + 0.32py + 6.76H_2O + 0.16O_2 \rightleftharpoons 0.68ch + 1.33ms + 1.06HF + 0.32S_2$	2.00
7.	34C-1377	$1.66ch + 2.98ms + 1.15sp + 0.17py + 2.34HF + 0.25O_2 \rightleftharpoons st + 3.90qtz + 2.72bi + 14.56H_2O + 0.32S_2$	1.29
8.	34C-1377	$8.62ky + 0.13ch + 1.40py + 1.16sp + 0.55H_2O + 1.34O_2 \rightleftharpoons st + 1.67qtz + 1.97S_2$	1.48
9.	34C-1377	$9.35ky + 0.24bi + 1.46py + 1.15sp + 1.87H_2O + 1.36O_2 \rightleftharpoons st + 1.47qtz + 0.26ms + 0.23HF + 2.04S_2$	1.49
10.	34C-1377	$4.36ch + 1.15sp + 8.23ms + 6.50HF + 0.35O_2 \rightleftharpoons st + 15.10ky + 7.53bi + 0.58py + 7.81qtz + 41.15H_2O$	0
11.	34C-1377	$5.87ch + 1.15sp + 11.11ms + 8.83HF + 0.69S_2 \rightleftharpoons st + 23.46ky + 10.17bi + 1.27py + 10.00qtz + 55.87H_2O$	∞

b. THE Si-Al-Fe-Mg-Mn-Zn-K-H-F-O-S SYSTEM

	Sample	Reaction	m[1]
12.	22A-1625	$0.08grt + 3.22ms + 1.38ch + 0.69py + 1.19sp + 1.99HF + 1.00O_2 \rightleftharpoons st + 2.63bi + 4.68qtz + 12.69H_2O + 1.28S_2$	1.28

[1] $m = \log f_{S_2} / \log f_{O_2}$. [2] Reaction solved by linear regression.

Coexisting phyllosilicate minerals at the Linda deposit show the normal sequence of F/OH partitioning: muscovite < chlorite < biotite. Magnesium number, X_{Mg} = Mg/(Mg + Fe), normally increases in pelitic rocks in the sequence: biotite < chlorite (Thompson 1976). In aluminous pelites, muscovite has been reported with X_{Mg} nearly equal to that of biotite (Novak & Holdaway 1981) or with lower X_{Mg} than biotite (Mengel & Rivers 1988). In the F-rich altered rocks of the Linda deposit, the X_{Mg} sequence is muscovite < chlorite < biotite, which thus matches the sequence of F–OH partitioning. The Fe–Mg partitioning coefficient between biotite and chlorite, K_D(bi–ch), shows a positive correlation with the F content of biotite (Fig. 5). As a result of Fe–F avoidance and the preference of F for biotite, the normally observed sequence of X_{Mg} is reversed, and Fe–Mg distribution is strongly composition-dependent. This critical observation has ramifications bearing on reaction topology.

Metamorphic Grade of the Linda Deposit

The Linda deposit occupies a small volume with respect to the scale of regional metamorphism. The altered rocks in the sample suite represent an even smaller volume, and it is reasonable to assume that all the samples underwent the same tectonometamorphic history.

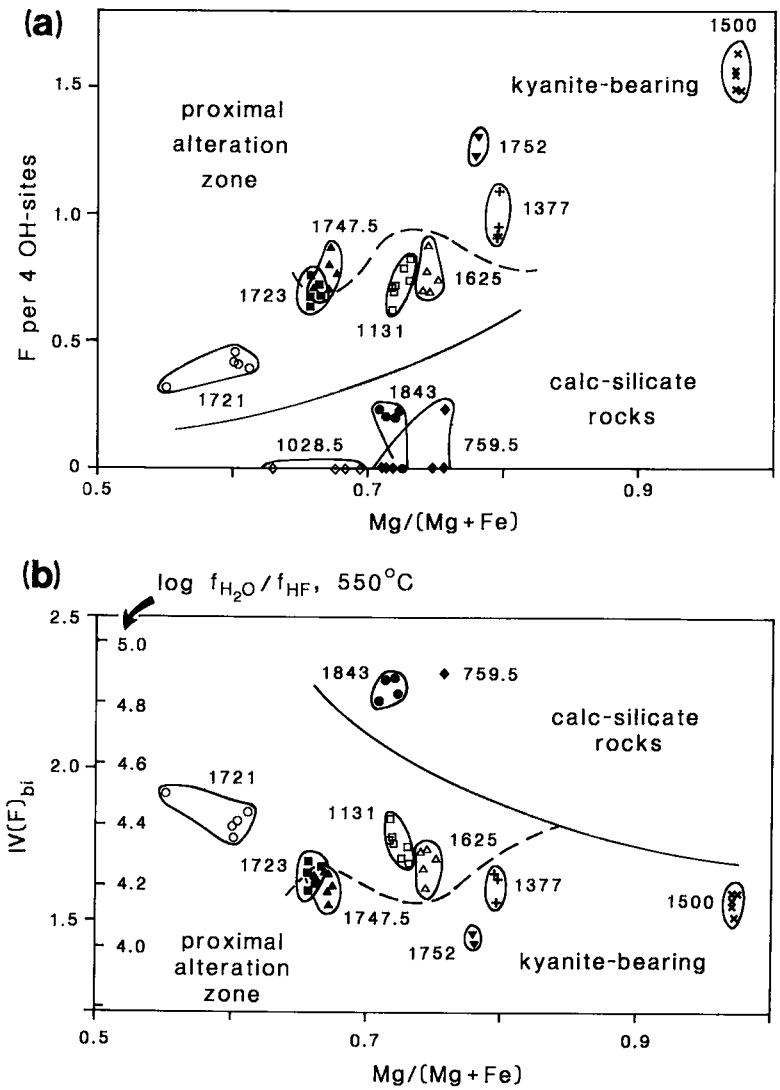

FIG. 4. Biotite compositions showing the relationships between Mg/(Mg + Fe) and F. In both figures, the solid line separates samples of the proximal zone of alteration from calc-silicate rocks, and the dashed line separates proximal-zone samples containing kyanite from those without kyanite. (a) F (per 4 OH sites) as a function of Mg/(Mg + Fe). Note the positive correlation, particularly for samples from the proximal zone of alteration. (b) F-intercept value, $IV(F)_{bi}$, determined by the method of Munoz (1984), as a function of Mg/(Mg + Fe). Values of log $f(H_2O)/f(HF)$ in coexisting fluids at an assumed temperature of 550°C are shown on the right-hand scale of the y axis.

Equilibrium assemblages

Mineral assemblages considered to represent equilibrium parageneses are summarized in Table 1; low-variance assemblages were used in balancing reactions (Table 3). Accessory minerals allowed the inference of supplementary information, for example the distribution of rutile and ilmenite as indicators of relative S_2 and O_2 fugacities.

Microstructural relationships between porphyroblasts and tectonic fabrics show that most porphyroblastic minerals crystallized during D_2.

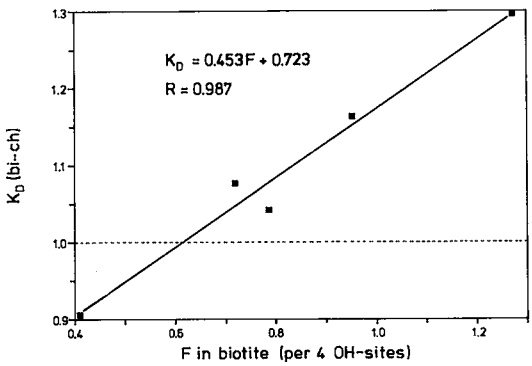

FIG. 5. Fe–Mg partitioning coefficient between biotite and chlorite, $K_D(bi\text{-}ch) = (Mg/Fe)_{bi}/(Mg/Fe)_{ch}$, as a function of F in biotite. There is a strong positive correlation, and the regression line passes through $K_D = 1.0$ at F = 0.61. Samples with $K_D < 1.0$ were not used in the construction of the grid in Figure 8.

This includes the assemblages biotite – kyanite and staurolite – anthophyllite, which represent the peak metamorphic grade achieved at the Linda deposit. Garnet and kyanite (without biotite) crystallized before D_2 and probably during D_1. Garnet rims were assumed to have re-equilibrated during D_2.

Chlorite and muscovite define S_1 schistosity; biotite and, less commonly, muscovite and chlorite show textures indicating crystallization or recrystallization during D_2. In general, where two textural generations of the same phyllosilicate mineral occur together, there was no systematic difference in their compositions. Apparently, phyllosilicate minerals showing textures typical of early crystallization re-equilibrated at higher grade.

Disseminated pyrite is abundant in all samples. Sphalerite, where present, varies from abundant to trace amounts. In general, even where present in small amounts, it has a wide distribution as fine

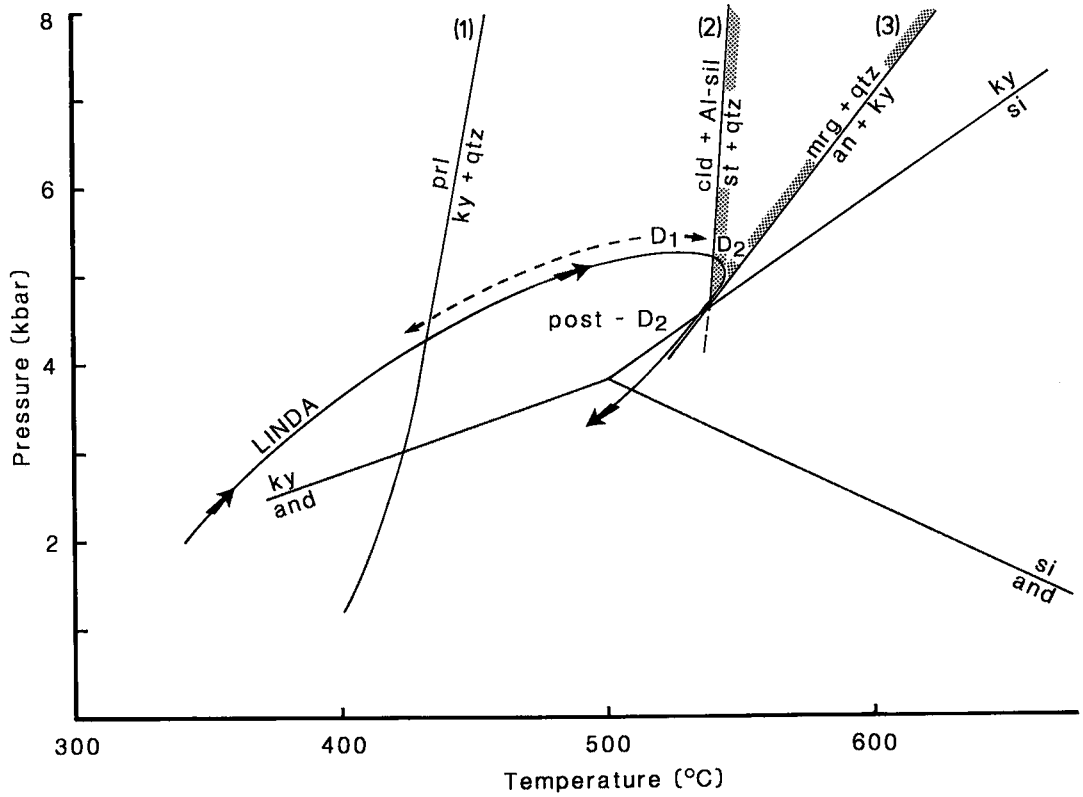

FIG. 6. Schematic pressure – temperature – deformation path followed by the Linda deposit. The low-grade kyanite-forming reaction accounts for syn-D_1 kyanite without biotite. Syn-D_2 minerals crystallized in the interval bounded by the stability limits of staurolite + quartz and margarite + quartz. Reaction 2 was determined for fixed bulk Fe/Mg of intermediate value (Hoschek 1967) and represents a narrow reaction-band. Sources of reaction data: 1 Kerrick (1968), 2 Hoschek (1967), 3 Storre & Nitsche (1974); stability fields of aluminosilicates: Holdaway (1971).

inclusions in syn-D_2 porphyroblasts and disseminated grains in the phyllosilicate matrix.

Constraints on pressure and temperature

Sphalerite geobarometry at the Linda deposit gives a pressure of 5.0 kbar [using the calibration function (standard error ±0.30 kbar) of Hutchison & Scott 1981], using the most Fe-rich sphalerite (Table 2e, 1723, 14.5 mol% FeS) associated with syn-D_2 porphyroblasts. This sphalerite coexists only with pyrite, and not with hexagonal pyrrhotite; therefore, 5.0 kbar is a maximum limiting pressure. Sphalerite inclusions in pre-D_2 garnet porphyroblasts have 13.3 to 13.8 mol% FeS (2 analyses), giving a pressure of 5.7 to 6.2 kbar, within 2σ error limits of 5 kbar. The matrix of this sample (1625) contains pyrite and monoclinic pyrrhotite. It is possible that the sphalerite equilibrated with pyrite and hexagonal pyrrhotite and was subsequently armored by garnet.

Syn-D_1 kyanite formed at low grade (Fig. 6). The coexistence of Fe-Mg staurolite (0.02% ZnO) and quartz at the Linda deposit gives an approximate lower limit for peak metamorphic grade, and the coexistence of margarite (Table 2a, 1500mrg) and quartz gives an upper limit. Syn-D_2 peak metamorphism is bracketed by these two assemblages (stippled reactions in Fig. 6) at a temperature of about 550°C. The intersection of the two limiting reactions gives a lower pressure limit of about 4.5 kbar. The minimum pressure is also constrained by the kyanite – sillimanite phase boundary.

The role of bulk-rock and fluid compositions

The variety of syn-D_2 parageneses at the Linda deposit is a function of variation in bulk-rock composition and metamorphic fluid composition, and not of a gradient in metamorphic grade. The temperature of about 550°C is reasonable for the chlorite – biotite – staurolite zone of regional metamorphism (Fig. 1). Garnet persisted in association with chlorite and muscovite by virtue of its high spessartine content (Table 2g).

In zincian bulk-rock compositions, the stability of staurolite is enhanced relative to binary Fe-Mg silicates. Staurolite is unique among common silicate minerals in that it has a tetrahedrally coordinated Fe-bearing site into which Zn partitions in preference to the octahedrally coordinated Fe-bearing sites of other Fe-Mg silicates (Holdaway *et al.* 1986, 1988). The incorporation of Zn into staurolite and gahnite allowed the assemblage staurolite – anthophyllite – gahnite to crystallize at the Linda deposit. Gahnite and staurolite in altered rocks must be treated as ternary Fe-Zn-Mg minerals.

The presence of F in biotite and amphibole allows the stable persistence of these minerals in granulite-facies terranes (Petersen *et al.* 1982, Valley *et al.* 1982). In the case of the Linda deposit, the incorporation of F into biotite allowed the crystallization of biotite + kyanite at a grade lower than that which would normally be expected in pelitic rocks. The influence of F on phase equilibria must be considered in prograde biotite-forming reactions.

Silicate – Oxide – Sulfide Equilibria

Model mineral reactions

Mineral assemblages considered to have equilibrated during D_2 peak metamorphism (Table 1) were modeled in the ten-component system Si-Al-Fe-Mg-Zn-K-H-F-O-S (Table 3a) using the mineral compositions determined for chlorite, biotite, muscovite, staurolite, gahnite and sphalerite (Table 2). Table 3b involves Mn as an additional component, and garnet as an additional phase. The presence of Na in biotite and muscovite was neglected.

At fixed temperature and pressure, samples containing seven mineral phases in the ten-component system will have a phase-rule variance of 3. If $f(H_2O)$ and $f(HF)$ are fixed, the variance will be 1, and the assemblage defines a reaction. The reaction can be balanced using the mineral compositions determined; the slope in log $f(S_2)$ – log $f(O_2)$ space is determined by the stoichiometry of the reaction. The slope is tangential to the reaction curve and applies to the particular mineral compositions from which it was determined.

Sample 34C-1377 contains eight mineral phases; thus, at fixed temperature, pressure, $f(H_2O)$ and $f(HF)$, the assemblage has a phase-rule variance of 0. The assemblage can be used to balance the bundle of univariant reactions radiating from the invariant point (Table 3a, Reactions 6–9). Reactions 10 and 11 conserve S_2 and O_2, respectively.

The reaction coefficients were determined exactly (in an algebraic sense) by formulating the mineral compositions as an array of linear mass-balance equations (Spear *et al.* 1982). The significance of the reaction coefficients was tested by the least-squares method on subsets of the minerals, by fitting the model to the composition of one mineral chosen as a dependent variable (Greenwood 1968, Spear *et al.* 1982). The procedure was iterated, taking each analyzed mineral in turn as the dependent variable. Residual values in excess of the propagated 2σ standard deviations, *i.e.*, $\sqrt{[\Sigma(coef-}$

ficient × $2\sigma)^2$], associated with the analyses were interpreted to indicate that the coefficients of the reaction are significant. Errors on the independent and dependent variables were taken into account by summing the squared weighted 2σ standard deviations for each element from each mineral analysis; we employed the regression coefficient of the mineral as a weighting factor.

Figure 7 is a schematic illustration of the principle, using Reaction 2 (Table 3a) as an example. As solved exactly, gahnite decomposition would occur in a three-phase triangle to sphalerite, staurolite and a small amount of kyanite. As solved by least squares in an algebraically overdetermined system (omitting kyanite), if the residual vector (R) does not exceed the 2σ error envelope, then decomposition in the three-phase triangle is indistinguishable from degenerate decomposition on the sphalerite – staurolite tie line. In the case of residual vectors in excess of 2σ errors, the coefficients of all phases would be significant.

The evaluation of the significance of reaction coefficients is critical in the case of reactions involving the decomposition of gahnite (22B–1723, 34–799, 22A–1638). The balanced reactions involve kyanite or an Fe–Mg phyllosilicate mineral, with relatively small coefficients. These coefficients are not significant within the 2σ errors, and the degenerate reactions were balanced by linear regression. The phase-rule variance of these reactions is not increased; within error limits, Al_2/Mg in gahnite and staurolite has a constant ratio and should be treated as one component. Error evaluation shows that the coefficient of chlorite in Reactions 1 and 8, and the coefficients of biotite and muscovite in Reaction 9, are significant in balancing the Mg component, and the coefficient of garnet in Reaction 12 is

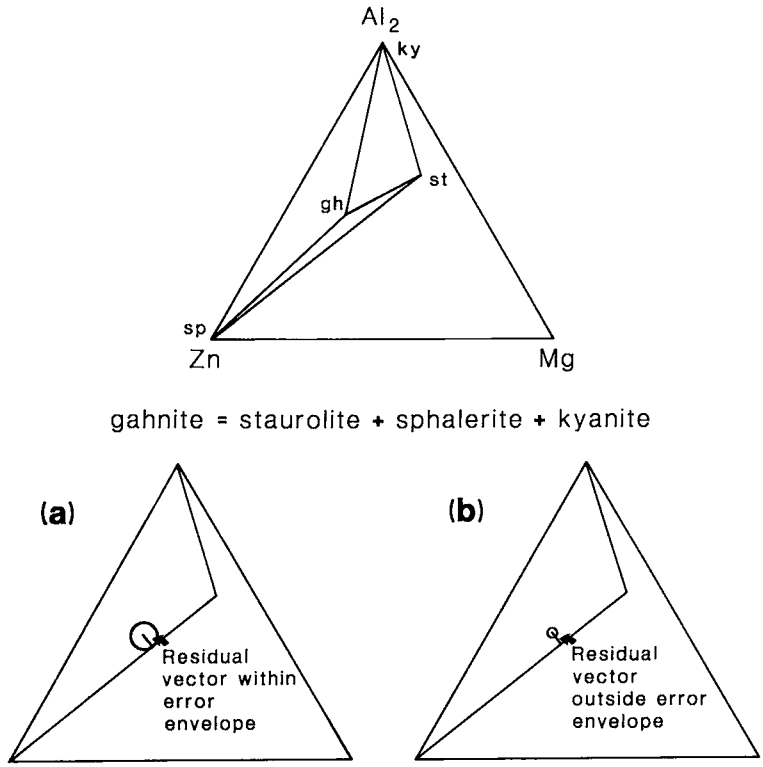

FIG. 7. Schematic illustration of the evaluation of the significance of reaction coefficients with respect to analytical uncertainty at the 2σ level. If the residual vector associated with least-squares solution of the mass balance, sphalerite + staurolite – gahnite = 0, lies within the 2σ error envelope, the coefficient for kyanite is not significant (a). If the residual vector exceeds the error envelope, the coefficient for kyanite is significant (b).

significant in balancing the Mn component. This also implies that the slopes of Reactions 8 and 9 are different.

Reactions 1 and 8 involve the same minerals, but with different compositions and, thus, the coefficients of the balanced reactions are different. The coefficients of O_2 and S_2 in these reactions were tested by varying the mineral compositions within their 2σ ranges of uncertainty. This procedure showed that the difference in the slopes, log $f(S_2)$/log$f(O_2)$ (see next section), exceeds the analytical error. Analytical error contributes an uncertainty of about ± 0.05 (or about 3%) to the slopes of these reactions.

Log $f(O_2)$ – log $f(S_2)$ petrogenetic grid

The model reactions (Table 3) involve oxidation and sulfidation, and each yields a reaction slope, m, in log $f(S_2)$ – log $f(O_2)$ coordinates. A Schreinemakers analysis of the reactions and slopes was used in the derivation of a petrogenetic grid in log $f(S_2)$ – log $f(O_2)$ coordinates, at fixed pressure and temperature (Fig. 8). The grid is projected

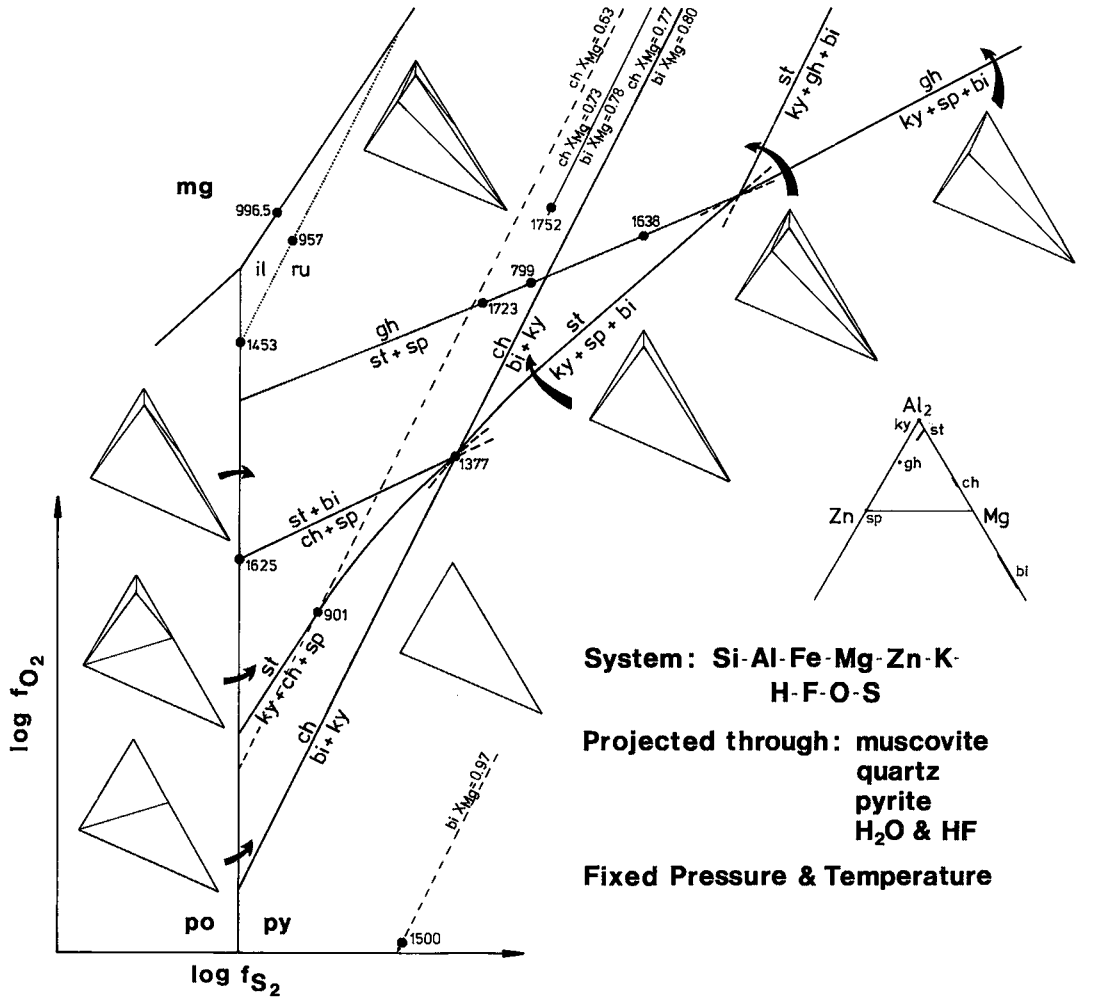

FIG. 8. Log $f(O_2)$ – log $f(S_2)$ petrogenetic grid derived by Schreinemakers analysis of the reactions in Table 3. The insets are projections onto the Zn–Al_2–Mg plane. Abbreviations: bi biotite, ch chlorite, gh gahnite, il ilmenite, ky kyanite, ru rutile, sp sphalerite, st staurolite.

through quartz, pyrite, muscovite of the analyzed composition, H_2O and HF. It is based only on samples showing a narrow range of log $f(H_2O)/f(HF)$, from 4.0 to 4.3 (Fig. 4), in fluids coexisting with biotite. In biotite-absent samples, log $f(H_2O)/f(HF)$ in the fluid is unknown.

The mineral compositions can be projected onto the Zn-Al_2-Mg plane. The choice of elemental components allows the projection of phase relations involving silicate, oxide and sulfide minerals. Each nondegenerate univariant reaction involves four phases in the subsystem Zn-Al_2-Mg. As previously discussed, gahnite compositions lie on the staurolite – sphalerite tie line, and the decomposition of gahnite is a degenerate reaction.

On Figure 8, the activity of FeO defines a family of contours with slopes of 2, determined by the stoichiometry of the reaction: $(FeO)_{silicate} + S_2 = FeS_2 + 0.5O_2$. The compositions of ternary Fe–Mg–Zn minerals (and sphalerite) vary along the univariant reactions; these reactions cross isopleths of the activity of FeO and Fe end-member in each mineral. The relative position of the sample points (Fig. 8) was constrained by the requirement that the analyzed silicate and oxide compositions become progressively more Fe-rich at lower fugacities of S_2. The compositional constraints define a unique solution of the phase relations for the samples involved.

The sulfidation of chlorite to biotite and kyanite occurs in a Zn-absent subsystem and provides a link to petrogenetic grids that are limited to binary Fe–Mg silicates (Nesbitt 1982, 1986a, b). The reaction slope is fixed at 2, as required by the stoichiometry of sulfidation, and the compositions of biotite and chlorite are constant. The reaction represents the intersection line of two continuous reactions of slope 2, involving the sulfidation of daphnite in chlorite [*i.e.*, $(da)_{ch} + S_2 = qtz + py + ky + 0.5O_2$] and the sulfidation of annite in biotite [*i.e.*, $(ann)_{bi} + ky + S_2 = qtz + py + ms + 0.5O_2$]. These continuous reactions define isopleths of Fe end-member activity, which decreases with increasing S_2 fugacity in the pyrite field. (Some isopleths of X_{Mg} are shown in Fig. 8, for example X_{Mg} in phlogopite of sample 1500.) The discontinuous reaction limits the most Mg-rich chlorite and the most Fe-rich biotite compositions coexisting with kyanite. (Note the limiting X_{Mg} values represented by sample 1377 in Fig. 8.)

The significance of fluorine

The consequences of the reversed Fe–Mg partitioning between biotite and chlorite, due to the presence of F, can be seen in reaction topology (Fig. 8); biotite, as the more magnesian mineral, is stable at higher S_2 fugacity than chlorite. In low-F or F-absent systems, the assemblage biotite + kyanite is sulfidized to a more magnesian chlorite (*e.g.*, Fig. 11 in Nesbitt 1986b).

In the petrogenetic grid (Fig. 8), $f(H_2O)$ and $f(HF)$ are assumed to be constant. The range of calculated log $f(H_2O)/f(HF)$ in fluids (Fig. 4) is consistent with minor variation, but it does not prove constant fugacities. Samples 1752 and 1377 contain chlorite – biotite – kyanite (Reactions 3 and 6, Table 3), with slightly different X_{Mg} in phyllosilicate minerals in each sample (Fig. 8). The divariance of the reaction may be due to slightly different log $f(H_2O)/f(HF)$ values, from about 4.0 in sample 1752 to 4.2 in 1377.

Sample 1747.5 contains kyanite + biotite, with biotite compositions much more Fe-rich than the limiting values in sample 1377 (Fig. 4). The mean composition in sample 1747.5 is 0.76 F (per 4 OH sites), Mg/Fe = 2.0 and corresponding log $f(H_2O)/f(HF)$ = 4.2. Figure 5 predicts "normal" Mg/Fe partitioning between chlorite and biotite for less than 0.61 F in biotite (per 4 OH sites), and Mg/Fe below about 2.4. Log $f(S_2)$, Mg/Fe, F and K_D(bi–ch) are all positively correlated; this suggests that a reversal in K_D(bi–ch) occurs in the petrogenetic grid (Fig. 8) at relatively low values of $f(S_2)$ regardless of constant $f(H_2O)$ and $f(HF)$. Such a reversal implies the possible reappearance of biotite + kyanite at lower log $f(S_2)$ (and more Fe-rich mineral compositions) and may account for the assemblage in sample 1747.5. The chlorite-bearing assemblages in samples 957 and 996.5 are inconsistent with biotite + kyanite in 1747.5. This problem is almost certainly related to variable $f(H_2O)$ and $f(HF)$; however, the available data do not allow conclusive resolution of the grid at low $f(S_2)$.

Pressure – Temperature Petrogenetic Grid for F-Rich Protolith

The reversal in Fe–Mg partitioning between biotite and chlorite has implications for the topology of P–T reaction grids. In Figure 9, the topology expected in pelitic rocks has been revised assuming a sequence of X_{Mg} in which biotite is more magnesian than chlorite. This topology is appropriate for a F-rich protolith, such as the altered rocks of the Linda deposit. The reaction of chlorite + staurolite to biotite + aluminosilicate, which is the biotite – aluminosilicate isograd reaction at Snow Lake (Fig. 1) and in pelitic rocks in general, does not occur. In the AFM plane, chlorite lies on the Fe-rich side of the biotite – aluminosilicate tie line; a discontinuous aluminosilicate-producing

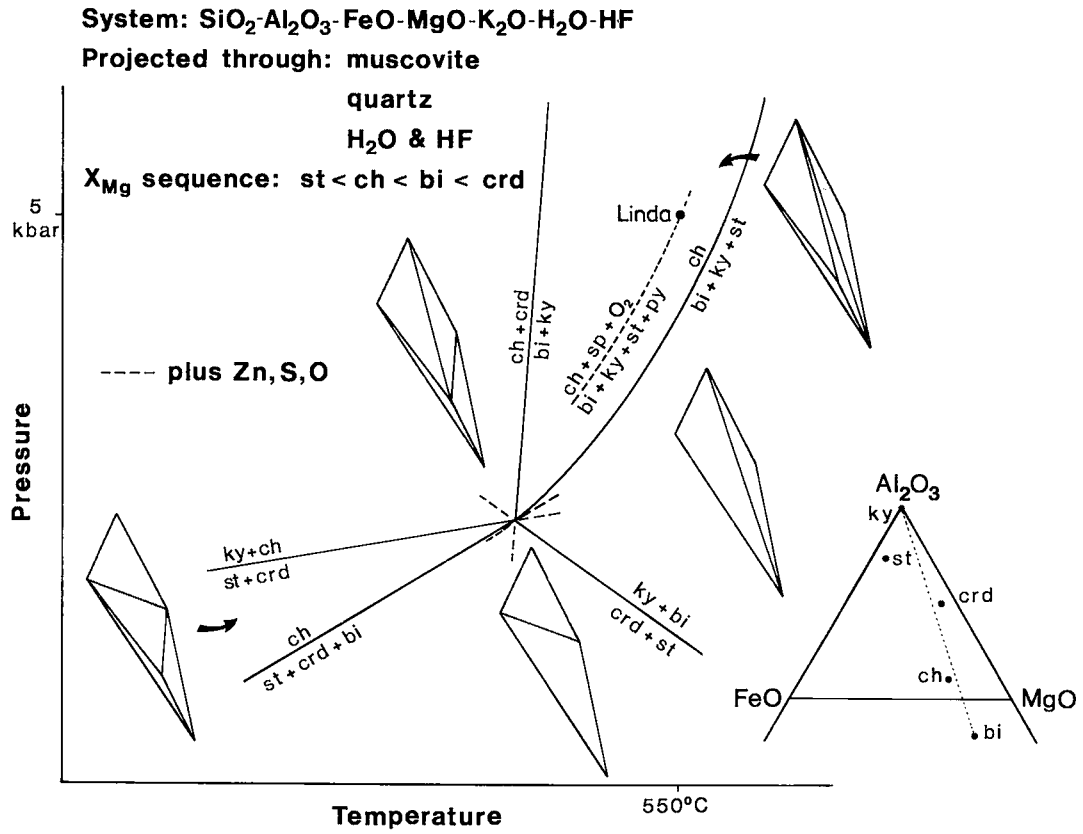

FIG. 9. Pressure – temperature grid for F-rich protolith in which biotite is more magnesian than chlorite. The insets are projections on to the AFM plane. The dashed line represents Reaction 10 (Table 3); the point labeled "Linda" corresponds to the gahnite-absent invariant point in Figure 8 (labeled "1377").

reaction would have to involve some more magnesian mineral, for example cordierite.

At a higher grade in a F-rich protolith, the P–T grid predicts chlorite decomposition within a three-phase triangle to biotite, staurolite and aluminosilicate. This four-phase assemblage is the same as that which defines the biotite – aluminosilicate isograd. This is a common assemblage at the Linda deposit, but with zincian staurolite present. The reaction that accounts for this assemblage in altered rocks involves the additional components Zn, S and O, and the additional mineral phases sphalerite and pyrite. Reactions 10 and 11 (Table 3a) are balanced using mineral compositions in sample 1377 and Reaction 10 is shown as a dashed line in Figure 9; the point (labeled "Linda") corresponds to the invariant point defined by this assemblage in $\log f(O_2)$ – $\log f(S_2)$ space in Figure 8 (labeled "1377"). In P–T space, the reaction is divariant as a function of O_2 and S_2 fugacities. If the activities of H_2O or HF also are not constant, the reaction is multivariant.

IMPLICATIONS FOR THE SNOW LAKE REGION

A temperature of about 550°C is reasonable for the chlorite – biotite – staurolite zone of regional metamorphism in pelitic rocks. The parageneses at the Linda deposit are consistent with this grade. Figure 10 compares the reactions in F-rich protolith with reactions in pelitic rocks as a function of grade. The left side of the figure is an isobaric section of the P–T grid in Figure 9. The biotite – aluminosilicate assemblage formed through different reactions in rocks of different bulk-composition, and these reactions occurred at different grades. In the F-rich protolith, the reaction occurred at lower temperature, within the stability field of kyanite. In pelitic rocks, the reaction occurred at higher grade, within the stability field of sillimanite. The reaction in pelitic rocks (Fig. 10) is the biotite – sillimanite isograd reaction proposed by Froese & Moore (1980) at Snow Lake (Fig. 1). The distribution of aluminosilicate polymorphs observed at Snow Lake supports the difference in

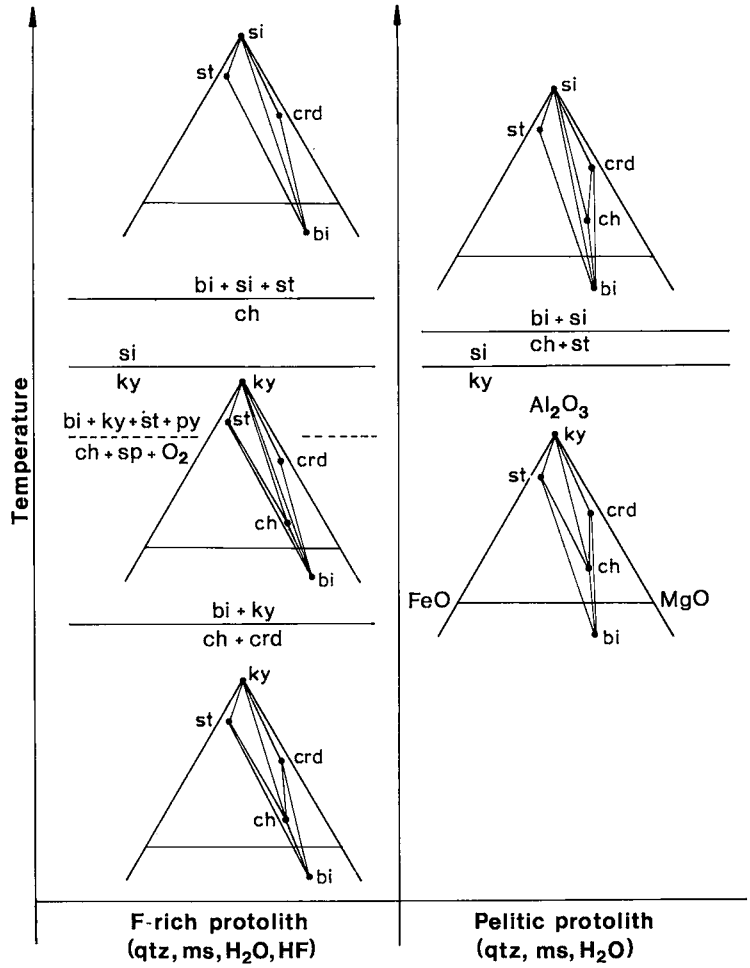

FIG. 10. Comparison of mineral assemblages in AFM projection between F-rich protolith and pelitic protolith, as a function of grade. The left side is an isobaric section through Figure 9 at 5 kbar, taking into account the kyanite – sillimanite transition at a grade slightly higher than that of the Linda deposit. Biotite – aluminosilicate forms through different reactions in the two bulk-rock compositions. The reactions occur at different grades, in the kyanite field in F-rich rocks, and in the sillimanite field in pelitic rocks. The biotite–sillimanite-forming reaction in pelitic protoliths corresponds to the isograd reaction at Snow Lake (Reaction 2, Fig. 1).

grade illustrated in Figure 10; biotite – sillimanite occurs in pelites, and biotite – kyanite is more common in altered rocks. The dashed reaction involves the additional components Zn, S and O, and is not definitive of grade if S_2 and O_2 fugacities (or HF) vary.

Concentrations of halogens have not been determined in micas from the Anderson Lake and Stall Lake mines (Fig. 1). The micas are likely to contain significant amounts of F; in this case, the biotite – aluminosilicate assemblage is not diagnostic of metamorphic grade. If the isograd were based solely on parageneses observed in pelitic metasedimentary rocks, it would lie further north and coincide closely with the leading edge of the McLeod Road thrust fault. A possible relationship between the fault and the isograd is being investigated by further work in the Snow Lake region.

CONCLUSIONS

Two major conclusions of general importance emerge from this study:

1. With appropriate restrictions, and in particular with a projection through pyrite, metamorphic assemblages in mineralized altered rocks can be projected into the subsystem Zn–Al_2–Mg. Different topologies are separated by reactions that form a grid on a log $f(O_2)$ – log $f(S_2)$ diagram. In contrast to earlier work, gahnite and staurolite can be treated as ternary Fe–Mg–Zn solutions, which is critical to the interpretation of their phase relations.
2. Despite the superficial similarity in their parageneses, P–T grids based on pelitic bulk-rock compositions are not appropriate for altered rocks. Direct comparison of assemblages in rocks of different bulk-composition will result in an incorrect interpretation of isograds. The incorporation of F into biotite expands the stability of biotite – aluminosilicate to lower grades. In the case of F-rich phlogopitic biotite, the biotite is more magnesian than coexisting chlorite and, consequently, the topology of reactions involving these minerals is modified. Petrogenetic grids appropriate for altered rocks can be developed; as stated by Eskola (1915), mineral parageneses "stand in definite relations to the chemical composition".

Acknowledgements

This study was part of the doctoral research of E. Zaleski under the supervision of Norman M. Halden, University of Manitoba. Falconbridge Limited and Minnova Incorporated provided access to drill core and to unpublished company maps and reports. Minnova provided funding for mineral analyses, and Falconbridge allowed the use of their office facilities at Snow Lake. Robert Spark assisted in the field. Thanks are due to T. Scott Ercit, Mineral Sciences Division, Canadian Museum of Nature, for instruction in the acquisition of high-quality mineral analyses. Discussions with Doreen Ames, Alan Bailes, Dugald Carmichael, Jim Franklin, Alan Galley and Roger Skirrow eventually germinated into ideas. The manuscript was improved by reviews from Robert F. Martin, Robert Tracy and anonymous reviewers. Funding from the Natural Sciences and Engineering Research Council was provided through their scholarship program and an operating grant to Norman Halden.

References

Bailes, A.H. (1987): GS-12 Chisel – Morgan Lakes project. *Manitoba Energy and Mines, Minerals Division, Report of Field Activities* **1987**, 70-79.

_____ (1988): GS-8 Chisel – Morgan Lakes project. *Manitoba Energy and Mines, Minerals Division, Report of Field Activities* **1988**, 53-61.

Bryndzia, L.T. & Scott, S.D. (1987): Application of chlorite – sulfide – oxide equilibria to metamorphosed massive sulfide ores, Snow Lake, Manitoba. *Econ. Geol.* **82**, 963-970.

Deer, W.A., Howie, R.A. & Zussman, J. (1966): *An Introduction to the Rock-Forming Minerals.* Longman Group Ltd., London.

Eskola, P. (1915): On the relations between the chemical and mineralogical composition in the metamorphic rocks of the Orijärvi region. *Bull. Comm. Géol. Finlande* **8**, 108-145 (English summary).

Foster, M.D. (1962): Interpretation of the composition and a classification of the chlorites. *U.S. Geol. Surv., Prof. Pap.* **414-A**.

Froese, E. (1971): The graphical representation of sulfide – silicate phase equilibria. *Econ. Geol.* **66**, 335-341.

_____ (1977): Oxidation and sulphidation reactions. *In* Application of Thermodynamics to Petrology and Ore Deposits (H.J. Greenwood, ed.). *Mineral. Assoc. Can., Short Course Handbook* **2**, 84-98.

_____ & Gasparrini, E. (1975): Metamorphic zones in the Snow Lake area, Manitoba. *Can. Mineral.* **13**, 162-167.

_____ & Moore, J.M. (1980): Metamorphism in the Snow Lake area, Manitoba. *Geol. Surv. Can., Pap.* **78-27**.

Frondel, C. & Ito, J. (1975): Zinc-rich chlorites from Franklin, New Jersey. *Neues Jahrb. Mineral. Abh.* **123**(2), 111-115.

Galley, A., Ames, D.E. & Franklin, J.M. (1988): Geological setting of gold mineralization, Snow Lake, Manitoba. *Geol. Surv. Can., Open-File Rep.* **1700**.

Grambling, J.A. (1983): Reversals in Fe–Mg partitioning between chloritoid and staurolite. *Am. Mineral.* **68**, 373-388.

Greenwood, H.J. (1968): Matrix methods and the phase rule in petrology. *XXIII International Geol. Congress* **6**, 267-279.

Guidotti, C.V. (1984): Micas in metamorphic rocks. *In* Micas (S.W. Bailey, ed.). *Rev. Mineral.* **13**, 357-467.

Gunow, A.J., Ludington, S. & Munoz, J.L. (1980): Fluorine in micas from the Henderson molybdenite deposit, Colorado. *Econ. Geol.* **75**, 1127-1137.

Holdaway, M.J. (1971): Stability of andalusite and

the aluminum silicate phase diagram. *Am. J. Sci.* **271**, 97-131.

_____, DUTROW, B.L. & HINTON, R.W. (1988): Devonian and Carboniferous metamorphism in west-central Maine: the muscovite – almandine geobarometer and the staurolite problem revisited. *Am. Mineral.* **73**, 20-47.

_____, _____ & SHORE, P. (1986): A model for the crystal chemistry of staurolite. *Am. Mineral.* **71**, 1142-1159.

HOSCHEK, G. (1967): Untersuchungen zum Stabilitätsbereich von Chloritoid und Staurolith. *Contrib. Mineral. Petrol.* **14**, 123-162.

HUTCHISON, M.N. & SCOTT, S.D. (1981): Sphalerite geobarometry in the Cu–Fe–Zn–S system. *Econ. Geol.* **76**, 143-153.

KERRICK, D.M. (1968): Experiments on the upper stability limit of pyrophyllite at 1.8 kilobars and 3.9 kilobars water pressure. *Am. J. Sci.* **266**, 204-214.

KRETZ, R. (1983): Symbols for rock-forming minerals. *Am. Mineral.* **68**, 277-279.

MENGEL, F. & RIVERS, T. (1988): Reversals in Fe-Mg distribution between muscovite and coexisting minerals in metapelites of the Ramah Group, northern Labrador: bulk compositional influences. *Geol. Assoc. Can. - Mineral. Assoc. Can., Program Abstr.* **13**, A84.

MOHR, D.W. & NEWTON, R.C. (1983): Kyanite – staurolite metamorphism in sulfidic schists of the Anakeesta Formation, Great Smoky Mountains, North Carolina. *Am. J. Sci.* **283**, 97-134.

MUNOZ, J.L. (1984): F–OH and Cl–OH exchange in micas with applications to hydrothermal ore deposits. *In* Micas (S.W. Bailey, ed.). *Rev. Mineral.* **13**, 469-493.

NESBITT, B.E. (1982): Metamorphic sulfide – silicate equilibria in the massive sulfide deposits at Ducktown, Tennessee. *Econ. Geol.* 77, 364-378.

_____ (1986a): Oxide – sulfide – silicate equilibria associated with metamorphosed ore deposits. I. Theoretical considerations. *Econ. Geol.* **81**, 831-840.

_____ (1986b): Oxide – sulfide – silicate equilibria associated with metamorphosed ore deposits. II. Pelitic and felsic volcanic terrains. *Econ. Geol.* **81**, 841-856.

NOVAK, J.M. & HOLDAWAY, M.J. (1981): Metamorphic petrology, mineral equilibria, and polymetamorphism in the Augusta quadrangle, south-central Maine. *Am. Mineral.* **66**, 51-69.

PETERSEN, E.U., ESSENE, E.J., PEACOR, D.R. & VALLEY, J.W. (1982): Fluorine end-member micas and amphiboles. *Am. Mineral.* **67**, 538-544.

SPEAR, F.S., RUMBLE, D., III & FERRY, J.M. (1982): Linear algebraic manipulation of N-dimensional composition space. *In* Characterization of Metamorphism through Mineral Equilibria (J.M. Ferry, ed.). *Rev. Mineral.* **10**, 53-104.

STORRE, B. & NITSCHE, K.-H. (1974): Zur Stabilität von Margarit im System $CaO–Al_2O_3–SiO_2–H_2O$. *Contrib. Mineral. Petrol.* **43**, 1-24.

THOMPSON, A.B. (1976): Mineral reactions in pelitic rocks. II. Calculation of some P–T–*X*(Fe–Mg) phase relations. *Am. J. Sci.* **276**, 425-454.

VALLEY, J.W., PETERSEN, E.U., ESSENE, E.J. & BOWMAN, J.R. (1982): Fluorphlogopite and fluortremolite in Adirondack marbles and calculated C–O–H–F fluid compositions. *Am. Mineral.* **67**, 545-557.

WALFORD, P.C. & FRANKLIN, J.M. (1982): The Anderson Lake mine, Snow Lake, Manitoba. *In* Precambrian Sulphide Deposits (R.W. Hutchinson, C.D. Spence & J.M. Franklin, eds.). *Geol. Assoc. Can., Spec. Pap.* **25**, 481-523.

ZALESKI, E. (1989): *Metamorphism, Structure and Petrogenesis of the Linda Volcanogenic Massive Sulphide Deposit, Snow Lake, Manitoba, Canada.* Ph.D. thesis, Univ. Manitoba, Winnipeg, Manitoba.

_____ & HALDEN, N.M. (1988): Reconstruction of synvolcanic alteration associated with the Linda massive sulphide deposit, Snow Lake, Manitoba. *Geol. Surv. Can., Pap.* **88–1C**, 73-81.

_____ & _____ (1991): Dynamometamorphism of the Linda volcanogenic massive sulphide deposit and its implications to the Snow Lake region, Manitoba, Canada. *Geol. Assoc. Can. – Mineral. Assoc. Can., Program Abstr.* **15**, A144.

Received May 29, 1990, revised manuscript accepted March 5, 1991.